AGU PUBLICATIONS

JGR

Journal of Geophysical Research: Space Physics

RESEARCH ARTICLE
10.1002/2014JA020319

Key Points:
- Thick PDLs form during CMEs
- Deep cusps during CMEs
- Reconnection negates induction currents

Correspondence to:
J. A. Slavin,
jaslavin@umich.edu

Citation:
Slavin, J. A., et al. (2014), MESSENGER observations of Mercury's dayside magnetosphere under extreme solar wind conditions, *J. Geophys. Res. Space Physics*, *119*, 8087–8116, doi:10.1002/2014JA020319.

Received 23 JUN 2014
Accepted 20 AUG 2014
Accepted article online 23 AUG 2014
Published online 8 OCT 2014

MESSENGER observations of Mercury's dayside magnetosphere under extreme solar wind conditions

James A. Slavin[1], Gina A. DiBraccio[1], Daniel J. Gershman[1,2], Suzanne M. Imber[1,3], Gang Kai Poh[1], Jim M. Raines[1], Thomas H. Zurbuchen[1], Xianzhe Jia[1], Daniel N. Baker[4], Karl-Heinz Glassmeier[5], Stefano A. Livi[6], Scott A. Boardsen[2,7], Timothy A. Cassidy[4], Menelaos Sarantos[2,8], Torbjorn Sundberg[9], Adam Masters[10], Catherine L. Johnson[11,12], Reka M. Winslow[11,12], Brian J. Anderson[13], Haje Korth[13], Ralph L. McNutt Jr.[13], and Sean C. Solomon[14,15]

[1]Department of Atmospheric, Oceanic and Space Sciences, University of Michigan, Ann Arbor, Michigan, USA, [2]Heliophysics Science Division, NASA Goddard Space Flight Center, Greenbelt, Maryland, USA, [3]Department of Physics and Astronomy, University of Leicester, Leicester, UK, [4]Laboratory for Solar and Atmospheric Physics, University of Colorado Boulder, Boulder, Colorado, USA, [5]Institut für Geophysik und Extraterrestrische Physik, Technische Universität Braunschweig, Braunschweig, Germany, [6]Southwest Research Institute, San Antonio, Texas, USA, [7]Goddard Planetary Heliophysics Institute, University of Maryland, Baltimore County, Baltimore, USA, [8]Goddard Earth Sciences and Technology Center, University of Maryland, Baltimore County, Baltimore, USA, [9]School of Physics and Astronomy, Queen Mary University of London, London, UK, [10]Blackett Laboratory, Imperial College, London, UK, [11]Department of Earth, Ocean, and Atmospheric Sciences, University of British Columbia, Vancouver, British Columbia, Canada, [12]Planetary Science Institute, Tucson, Arizona, USA, [13]The Johns Hopkins University Applied Physics Laboratory, Laurel, Maryland, USA, [14]Department of Terrestrial Magnetism, Carnegie Institution of Washington, Washington, District of Columbia, USA, [15]Lamont-Doherty Earth Observatory, Columbia University, Palisades, New York, USA

Abstract The structure of Mercury's dayside magnetosphere is investigated during three extreme solar wind dynamic pressure events. Two were the result of coronal mass ejections (CMEs), and one was from a high-speed stream (HSS). The inferred pressures for these events are ~45 to 65 nPa. The CME events produced thick, low-β (where β is the ratio of plasma thermal to magnetic pressure) plasma depletion layers and high reconnection rates of 0.1–0.2, despite small magnetic shear angles across the magnetopause of only 27 to 60°. For one of the CME events, brief, ~1–2 s long diamagnetic decreases, which we term cusp plasma filaments, were observed within and adjacent to the cusp. These filaments may map magnetically to flux transfer events at the magnetopause. The HSS event produced a high-β magnetosheath with no plasma depletion layer and large magnetic shear angles of 148 to 166°, but low reconnection rates of 0.03 to 0.1. These results confirm that magnetic reconnection at Mercury is very intense, and its rate is primarily controlled by plasma β in the adjacent magnetosheath. The distance to the subsolar magnetopause is reduced during these events from its mean of 1.45 Mercury radii (R_M) from the planetary magnetic dipole to between 1.03 and 1.12 R_M. The shielding provided by induction currents in Mercury's interior, which temporarily increase Mercury's magnetic moment, was negated by reconnection-driven magnetic flux erosion.

1. Introduction

Magnetic field measurements by the MErcury Surface, Space ENvironment, GEochemistry, and Ranging (MESSENGER) spacecraft show that Mercury's internal magnetic field is highly dipolar, is closely aligned with the planet's rotation axis, and has the same polarity as that of Earth, but with an offset northward from the planetary center of ~0.2 R_M, where R_M is Mercury's radius [*Anderson et al.*, 2008, 2010, 2011a, 2012; *Alexeev et al.*, 2008, 2010; *Johnson et al.*, 2012]. An illustration of the low-altitude portion of MESSENGER's orbit against Mercury's dayside magnetic field is shown in Figure 1a. The MESSENGER trajectory depicted is representative of the intervals considered in this paper, with the orbital periapsis on the dayside and the orbital plane making a small angle to the noon-midnight plane. These intervals are termed "hot seasons" because MESSENGER experiences its highest thermal input from the planet during such orbits. The mean distance from Mercury's offset dipole to the subsolar magnetopause (represented in the figure approximately by the outermost closed magnetic field line), on the basis of Mariner 10 and MESSENGER observations, is ~1.45 R_M [*Ness et al.*, 1976; *Slavin et al.*, 2010a; *Winslow et al.*, 2013].

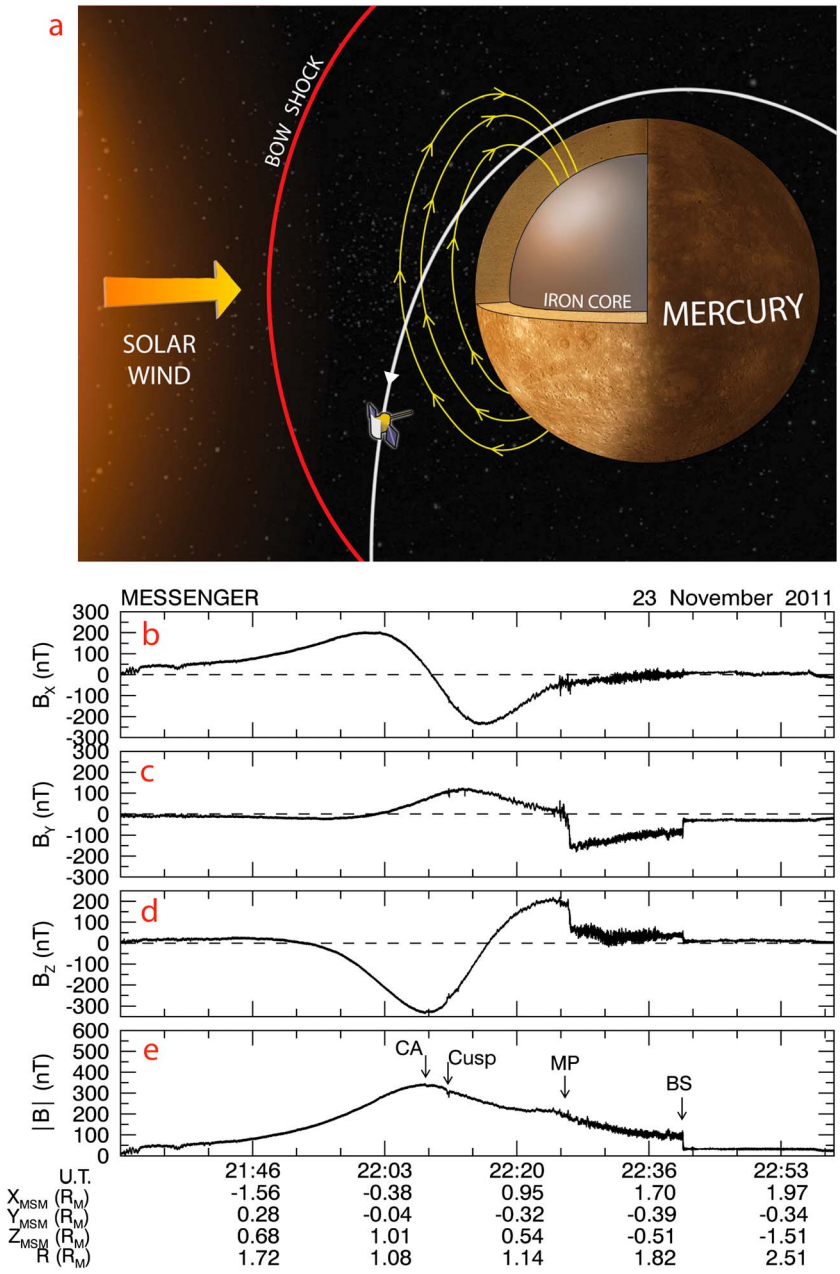

Figure 1. (a) Schematic view of a portion of Mercury's magnetosphere, showing the bow shock (red), some dayside magnetic field lines (yellow), and a cutaway view of Mercury's large iron core. The outermost field line shown lies at a distance of ~(1.4–1.5) R_M sunward of the planetary magnetic dipole, whereas the nose of the bow shock is at ~(1.9–2.0) R_M [*Winslow et al.*, 2013]. During the period for which orbits have been analyzed here, the MESSENGER spacecraft orbit (white) had a periapsis or closest approach (CA) altitude that ranged from 200 to 500 km and an inclination of ~82.5°. (b–e) Magnetic field measurements (20 s^{-1} sampling rate) taken during a typical MESSENGER periapsis pass late on 23 November 2011; shown are B_X, B_Y, B_Z, and B. Bow shock (BS) and magnetopause (MP) crossings are labeled, and the distance R from the planetary magnetic dipole is indicated.

MESSENGER Magnetometer (MAG) observations [*Anderson et al.*, 2007] from a rather quiet pass that occurred late on 23 November 2011 (after one of the extreme events analyzed in this paper) are shown in Figure 1. Full-resolution (20 s^{-1}) MAG measurements of the local magnetic field **B** are displayed in Mercury solar magnetospheric (MSM) coordinates [*Anderson et al.*, 2012]. In this coordinate system, the X_{MSM} axis is directed from Mercury's offset magnetic dipole toward the center of the Sun, the Z_{MSM} axis is normal to Mercury's orbital plane and points toward the north celestial pole, and the Y_{MSM} axis completes the

right-handed system with the positive direction oriented opposite to orbital motion. The interval displayed begins with MESSENGER having exited the plasma sheet, moved into the northern lobe of the near tail, and begun its periapsis pass. The magnetic field magnitude smoothly increased as MESSENGER traveled toward Mercury's north magnetic pole, reaching a maximum magnetic field strength of 341 nT at 22:08:24 UTC, when the altitude was 450 km. The polarity of B_X reversed near the maxima in the field magnitude and southward (i.e., inward) B_Z.

The northern magnetospheric cusp (see Figure 1e), as expected, was encountered over the dayside hemisphere at high latitudes. On the occasion shown in Figure 1, it was traversed just after MESSENGER's closest approach (CA) to the surface at an altitude of 402 km. The cusp may generally be identified by the diamagnetic effect of the solar wind plasma entering directly from the magnetosheath [*Winslow et al*., 2012]. The cusp, at ~ 22:11:20 UTC in Figure 1e, however, is barely discernable because the diamagnetic decrease in total magnetic field intensity was small. As reported by *Winslow et al*. [2012] and *Raines et al*. [2013, 2014], the amount of plasma in the cusp region and hence its diamagnetic effect are highly variable.

The magnetopause crossing at 22:26:40 UTC is apparent in Figure 1 on the basis of the rotation of the magnetic field from its dipole configuration to the draped interplanetary magnetic field orientation in the magnetosheath. In contrast to Earth and the outer planets, the magnetosheath at Mercury is usually low in the ratio β of plasma thermal to magnetic field pressure, and a plasma depletion layer (PDL) is adjacent to the magnetopause [*Gershman et al*., 2013]. These conditions were reflected in the very modest decrease in magnetic field intensity (Figure 1) as MESSENGER passed from the magnetosphere into the subsolar magnetosheath. MESSENGER exited the magnetosheath through the bow shock (BS) at 22:40:57 UTC.

Siscoe and Christopher [1975] were the first to take a long series of measurements of solar wind ram pressure collected at 1 AU, scale it inward to Mercury's orbit by $1/r^2$ to account for the increase in solar wind density with decreasing heliocentric distance r, and then use the planetary dipole moment inferred from Mariner 10 observations [*Ness et al*., 1974] to compute the distribution of solar wind standoff distances for the nose of the magnetopause. They found that for almost all solar wind pressure conditions the magnetopause stood off from Mercury's surface. However, the *Siscoe and Christopher* [1975] analysis considered only the effect of solar wind dynamic pressure and planetary dipole strength, but not the effects of dayside magnetic reconnection or electromagnetic induction in the planetary interior.

Observations at Earth have shown that magnetic reconnection removes magnetic flux from the dayside magnetosphere and transfers it to the magnetotail, thereby eroding the dimensions of the forward magnetosphere [*Aubry et al*., 1971; *Holzer and Slavin*, 1978; *Sibeck et al*., 1991]. The magnetic flux transferred to the nightside magnetosphere may immediately undergo reconnection or be stored and later returned to the dayside in an intense episode of reconnection in the tail [*Caan et al*., 1977; *Holzer and Slavin*, 1978; *Milan et al*., 2004; *Huang et al*., 2009]. Such tail loading and unloading events are termed magnetospheric substorms [*McPherron et al*., 1973; *Baker et al*., 1996]. Empirically, the timescale for substorms corresponds approximately to one complete circulation cycle of plasma and magnetic flux, first from the reconnection site at the dayside magnetopause to the reconnection site in the nightside cross-tail current sheet, and then back to the forward magnetosphere. This reconnection-driven circulation is called the Dungey cycle [*Dungey*, 1961] and has a timescale of ~1 to 3 h at Earth [*Tanskanen*, 2009] but only ~1 to 3 min at Mercury [*Siscoe et al*., 1975; *Slavin et al*., 2009, 2010a, 2012a; *DiBraccio et al*., 2013]. At other times, especially when solar wind conditions produce intense but steady reconnection at the dayside magnetopause, the circulation or convection of magnetic flux and plasma in Earth's magnetosphere occurs in a relatively continuous manner. This behavior is termed steady magnetospheric convection (SMC) [*Sergeev et al*., 1996; *Tanskanen et al*., 2005]. Evidence for both modes of convection, substorms and SMCs, has been reported for different intervals at Mercury [*Slavin et al*., 2009, 2012b; *Sundberg et al*., 2012].

Low-latitude reconnection at Earth is strongly controlled by the magnetic shear angle across the magnetopause, i.e., the angle between the magnetic field vectors in the magnetosheath and magnetosphere adjacent to the magnetopause. In particular, the highest rates of reconnection are observed for the largest shear angles when the interplanetary magnetic field (IMF) has a strong southward component [*Reiff and Luhmann*, 1986; *Mozer and Retinò*, 2007; *Fuselier and Lewis*, 2011]. This behavior is called the "half-wave rectifier effect" [*Burton et al*., 1975]. The ultimate reason that reconnection at Earth requires large shear angles, ~ 90 to 270°, is the high-average Alfvénic Mach number M_A at 1 AU, i.e., ~ 6–12 [*Slavin et al*., 1984; *Sarantos et al*., 2007]. These high Mach numbers

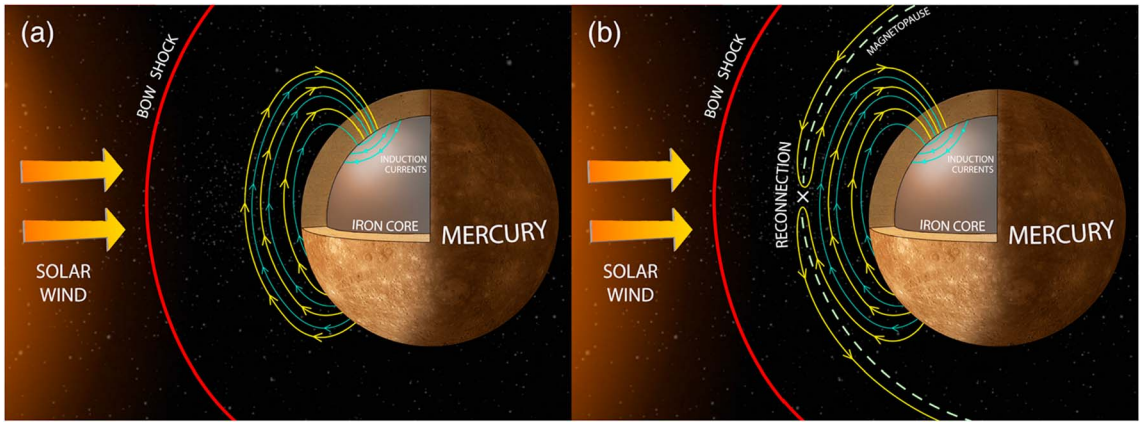

Figure 2. (a) Increases in solar wind pressure drive induction currents (green loops) at the top of Mercury's large iron core. The sense of these currents is to oppose the compression of the intrinsic magnetic field (yellow) by generating additional magnetic flux (green field lines) that, when added to the intrinsic flux, acts to balance the increased solar wind pressure. (b) Magnetic reconnection between the interplanetary magnetic field and the intrinsic planetary magnetic field opposes the effectiveness of induction by removing magnetic flux from the dayside magnetosphere and transporting it to the tail.

result in a high-β magnetosheath and generally thin, weak PDLs adjacent to the magnetopause [*Zwan and Wolf*, 1976; *Crooker*, 1979]. Even when solar wind conditions produce a well-developed layer of plasma-depleted flux tubes draped about the dayside magnetopause at Earth, the onset of reconnection often leads to PDL dissipation because of the high flux transfer rates that ensue [*Anderson et al.*, 1997]. The typically high-β magnetosheath at Earth causes the magnetic fields on either side of the magnetopause to differ greatly in magnitude. Under these circumstances, reconnection is possible only for large shear angles, typically greater than 90° [see *Sonnerup*, 1974]. In contrast, the presence of a strong PDL in the inner magnetosheath naturally leads to magnetic fields of similar magnitude on either side of the magnetopause. For the low-β magnetosheath and well-developed PDL observed at Mercury [*Gershman et al.*, 2013], the near equality of the magnetic field on either side of the magnetopause (see Figure 1) will allow reconnection to occur for arbitrarily low shear angles such as observed, for example, across heliospheric current sheets where the magnetic fields are also nearly equal on both sides [*Gosling et al.*, 2005; *Phan et al.*, 2005].

Slavin and Holzer [1979] were the first to consider the effect of erosion on Mercury's magnetosphere. They assumed the terrestrial style half-wave rectifier reconnection model, but they increased the efficiency (i.e., the fraction of the flux of southward IMF incident upon the dayside magnetopause that undergoes reconnection) from the Earth value by a factor of ~3 to account for the enhanced Alfvén speeds in the inner solar system. They argued that these high Alfvén speeds would ultimately lead to correspondingly higher absolute inflow speeds to the diffusion region, and, hence, higher reconnection rates, as well as an overall increase in the fraction of the incident IMF flux that reconnects with the planetary magnetic field. Further, they suggested that the expected low electrical conductance of the planetary regolith should greatly reduce the retarding effects of line tying, i.e., field-aligned currents that limit the cross-magnetospheric electric potential drop and the rate of magnetospheric convection [*Hill et al.*, 1976]. With these considerations they estimated that erosion could reduce the altitude of the dayside magnetopause at Mercury by several tenths of a Mercury radius. Given the mean subsolar magnetopause altitude of only ~(0.4–0.5) R_M, *Slavin and Holzer* [1979] concluded that reconnection, especially during intervals of enhanced solar wind pressure, might erode the magnetopause down to the surface.

Mercury has the highest uncompressed density of planetary bodies in our solar system because of its ~2000 km radius, iron-rich, electrically conducting core [*Smith et al.*, 2012]. As a result, changes in the external magnetic field are estimated to take of order 10^4–10^5 years to diffuse to the center of the planet [*Glassmeier*, 2000; *Grosser et al.*, 2004]. Given the short timescales for solar wind pressure increases, i.e., durations of several minutes to days, Mercury's core will react as a perfectly electrically conducting sphere with respect to all changes in solar wind pressure. Changes in the magnetic field normal to the surface of the large conducting core will generate currents according to Faraday's law that oppose the change in the magnetic field, as shown in Figure 2a [*Hood and Schubert*, 1979; *Suess and Goldstein*, 1979; *Glassmeier et al.*, 2007]. The magnetic flux sandwiched between the magnetopause and the surface of the core can still be compressed, but it will diffuse into the core only on very long timescales. The *Hood and Schubert* [1979], *Suess and Goldstein* [1979], and *Glassmeier et al.* [2007]

Table 1. Extreme Solar Wind Events

Year	DOY[a]	IMF[b]: B_X' B_Y' B_Z' (nT)	V_r[c] (km/s)	P_{sw}[d] (nPa)
2011	327	(7.66, 92.0, 31.9)	450	51.0
2012	129	(−2.01, 20.1, −9.50)	500	65.1
2012	132[e]	(13.0, −9.51, −0.20)	425	53.0
				48.8
				48.6
				44.1
				44.3

[a]Day of the year.
[b]IMF averaged over 20 min upstream of outbound bow shock.
[c]FIPS measurement immediately upstream of bow shock.
[d]Determined from equation (1).
[e]Pressure determined for five of the multiple magnetopause crossings.

models predict that the subsolar magnetopause altitude will remain at or above ~0.2 R_M for even the highest anticipated solar wind dynamic pressures at Mercury.

We have surveyed the MESSENGER hot season orbits in 2011 and 2012 for which the outbound magnetopause crossing(s) occurred within 1 h of local noon to identify intervals when Mercury's magnetosphere was subjected to extremely high solar wind dynamic pressure. For these hot season orbits, the spacecraft passed through the nightside plasma sheet, the northern cusp, and the subsolar magnetopause just before and during each periapsis pass (Figure 1a). Only three passes were identified for which the magnetic field just inside the magnetopause exceeded 300 nT. We have analyzed MESSENGER measurements for these events to infer the upstream dynamic pressure and the response of the dayside magnetosphere, and to assess the relative roles of magnetic reconnection and currents induced in the interior of the planet to standing off the solar wind under these extreme conditions. The choice of 300 nT is somewhat arbitrary, but it is a factor of 2 to 3 greater than the typical intensity of the magnetic field in the subsolar magnetosphere [*DiBraccio et al*., 2013; *Winslow et al*., 2013], implying solar wind ram pressures that are a factor of 4 to 9 greater than normal. The results confirm that magnetic reconnection at Mercury is very intense and that its rate is primarily controlled by plasma β in the adjacent magnetosheath. The additional shielding provided by the induction currents, which effectively increase the magnetic moment of Mercury when solar wind pressure increases, is found to be largely negated by reconnection-driven erosion. Indeed, an average magnetopause surface passing through the lowest-altitude magnetopause crossing, which had the highest inferred solar wind pressure and reconnection rate, intersected the planetary surface in the southern hemisphere where the surface magnetic field is weakest. The results of our analyses indicate that not only high-intensity reconnection but also magnetosphere-core coupling must be included in global models of Mercury's magnetosphere during extreme solar wind pressure conditions.

2. Overview of Extreme Solar Wind Events

The MESSENGER spacecraft entered orbit about Mercury [*Solomon et al*., 2001] on 18 March 2011. MESSENGER remained in this high-inclination, highly eccentric (~200 × 15,000 km altitude) orbit until 16 April 2012, when the apoapsis was decreased and the orbital period reduced to 8 h. For our purposes, the primary difference between these two orbits is that in the 12 h orbit the spacecraft crossed the dayside magnetopause at lower latitudes and the plasma sheet farther down the tail than in the 8 h orbit.

Typical values of the magnetic field just inside the dayside magnetopause are ~150 nT [*DiBraccio et al*., 2013; *Winslow et al*., 2013], corresponding to solar wind ram pressures of ~10 nPa. For the extreme solar wind events identified for this study we require that the magnetic field just inside the subsolar magnetopause exceeds 300 nT, implying a minimum solar wind pressure of ~20 nPa. As discussed above, this threshold is arbitrary, but it is the highest pressure for which multiple orbits could be found during which MESSENGER's orbital plane made a small angle to the noon-midnight plane and measurements were acquired in the key regions of the magnetosphere. As noted above, only three MESSENGER periapsis passes through Mercury's subsolar region met this requirement (Table 1). They occurred on 23 November 2011, 8 May 2012, and 11 May 2012. The magnetopause locations seen on these MESSENGER orbits are compared with the average location of the magnetopause [*Winslow et al*., 2013] in solar wind-aberrated (primed) MSM coordinates in Figure 3. The coordinates have been aberrated by Mercury's orbital velocity so that a 400 km/s solar wind directed radially outward from the Sun moves in the $-X'_{MSM}$ direction. As expected for such high dynamic pressures, the magnetopause crossings for these orbits were all displaced substantially inward from the mean boundary model and lay very close to Mercury's surface. The effect of the northward offset in Mercury's dipole magnetic

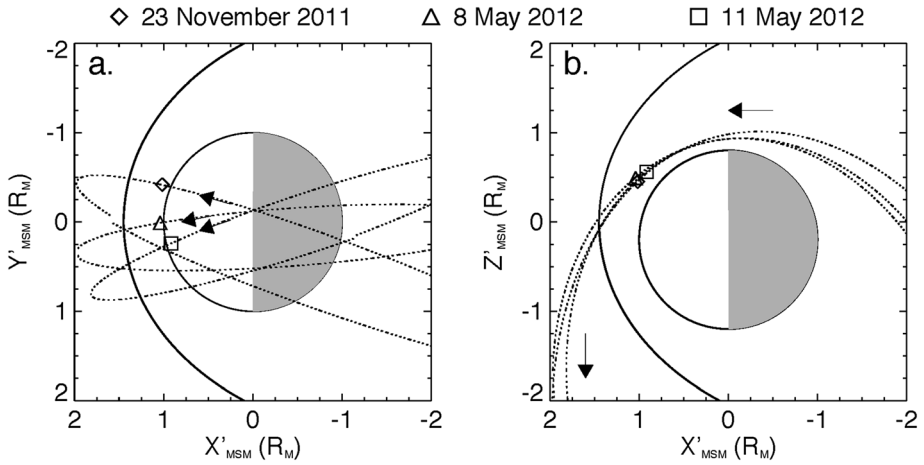

Figure 3. The three MESSENGER orbits of this study projected onto the aberrated MSM (a) *Y′*–*X′* and (b) *Z′*–*X′* planes relative to Mercury's surface (circle) and its mean magnetopause (solid line) [*Winslow et al*., 2013]. Note the displacement in Figure 3b of the magnetopause relative to the planetary center because of the northward offset of the magnetic dipole by ~0.2 R_M. The extreme compression of the dayside magnetosphere on these passes is evident in the very low altitudes of the magnetopause crossings on 23 November 2011, 8 May 2012, and 12 May 2012 (diamonds, squares, and triangles, respectively). The 23 November 2011 (DOY 327) orbit is before the reduction in orbital period from 12 h to 8 h, whereas the other two are afterward. Note that the 23 November 2011 trajectory arcs farther downstream to intersect the midplane of the tail at greater distances than for the 8 h orbits.

field is clearly evident in the closeness of the model magnetopause to the surface, especially in the southern hemisphere where the planetary field is weakest. We discuss the possible compression of the magnetopause to the surface in the southern hemisphere in section 6.

An ideal magnetohydrodynamic simulation called ENLIL [*Odstrcil et al*., 2004; *Toth and Odstrcil*, 1996] provides global context for these extreme pressure events. The simulation is based on the Wang-Sheeley-Arge (WSA) model of the coronal magnetic field derived by ground-based observations of the photospheric magnetic field gathered over a solar rotation [*Arge et al*., 2004]. Details of the WSA-ENLIL model, as applied to the inner heliosphere in support of MESSENGER, have been given by *Baker et al*. [2009, 2013]. Coronal mass ejections (CMEs) are included by means of the "cone model," whereby the CME is usually assumed to start near 21.5 solar radii and then propagate outward with a constant angular extent and radial velocity. The properties of a specific CME, and its "cone," are determined from remote observations, usually acquired by the coronal imagers on the Solar TErrestrial RElations Observatory (STEREO) spacecraft [*Xie et al*., 2004].

On 23 November 2011, MESSENGER started its first periapsis pass of the day moving northward and sunward to cross the downstream bow shock and pass from the solar wind into the magnetosheath at 05:03:54 UTC. Shortly thereafter, an interplanetary shock wave passed over MESSENGER at 05:19:40 UTC. After passing through periapsis and exiting the magnetosphere through the dayside magnetopause and the bow shock, MESSENGER measured an IMF that was oriented largely in the $+Y_{MSM}$ direction; $B_X = 7.65$ nT, $B_Y = 92.0$ nT, $B_Z = 31.9$ nT, and $B = 98.2$ nT (Table 1). This IMF direction represents a 20 min average, but the magnetic field draping pattern in the near-Mercury magnetosheath appears to have been relatively stable during this event. An upstream solar wind speed of 450 km s^{-1} (Table 1) was derived from measurements acquired by MESSENGER's Fast Imaging Plasma Spectrometer (FIPS) [*Andrews et al*., 2007] using the methodology detailed by *Gershman et al*. [2013], but density could not be recovered. The state of compression of the dayside magnetosphere can be analyzed to infer solar wind dynamic pressure, as described below.

Equatorial views of the solar wind velocity V_r and the density n, the latter multiplied by the square of radial distance (in units of AU) from the center of the Sun to detrend for the decrease in density with increasing distance, are displayed in Figure 4. The views are snapshots at 24:00 UTC on 23 November 2011 after the CME passed over Mercury. The solar wind speed (Figure 4a) shows the CME near the trailing edge of a higher-speed stream. The solar wind density (Figure 4b) depicts the expected compression signatures of the interaction region where the higher-speed stream overtakes the slower solar wind. The CME does not stand out in the velocity display because its speed is only ~450 km/s, but it is very clear in the density display because of the high-density compression signature as it overtakes the slower upstream solar wind.

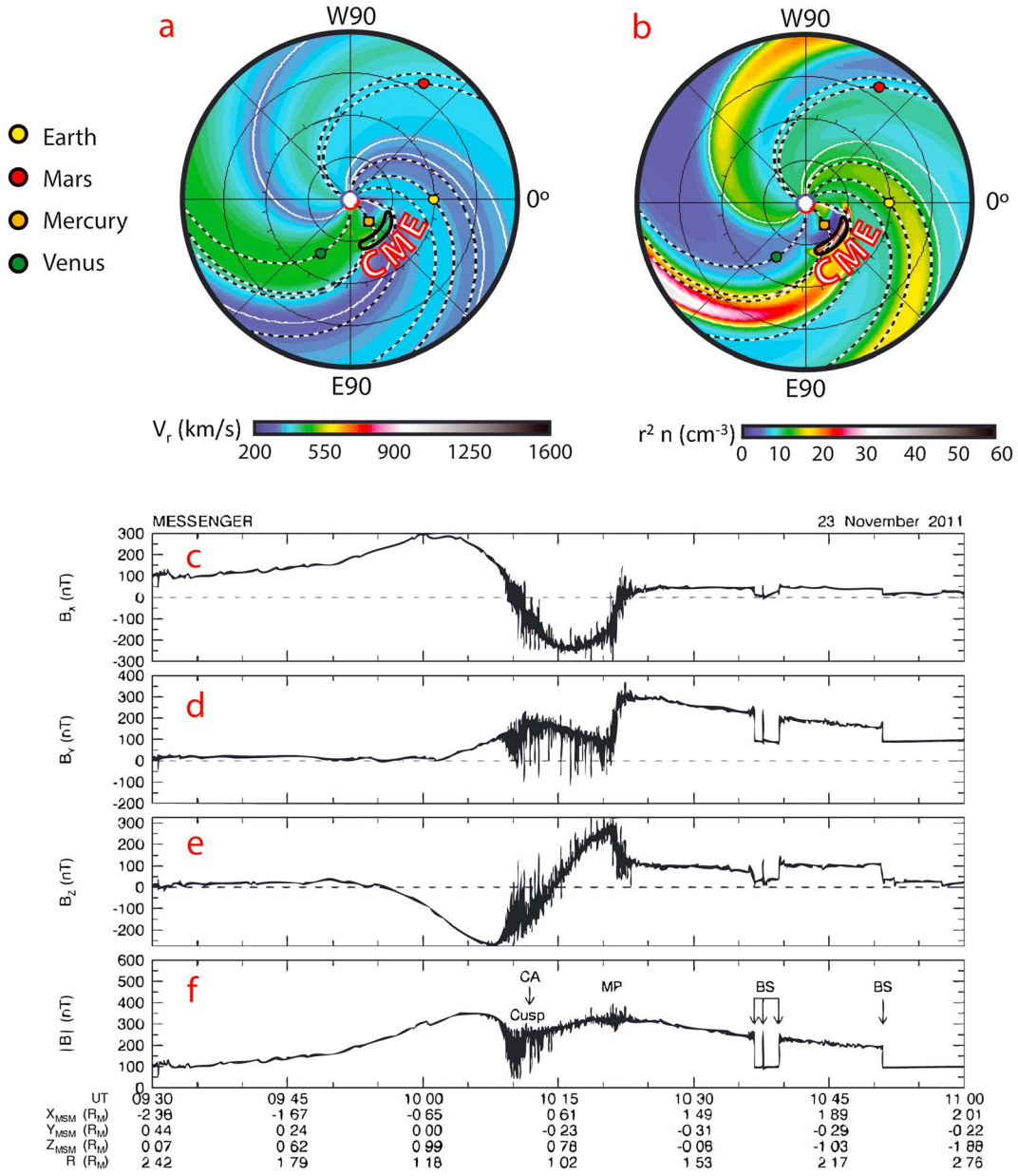

Figure 4. ENLIL-WSA models of (a) solar wind speed V_r and (b) the product of solar wind density n and the square of distance r from the Sun in AU for 23 November 2011 at 24:00 UTC. The center of a coronal mass ejection impacted Mercury and its magnetosphere (yellow circle). The locations of Earth, Venus, and Mercury are all indicated by small colored dots. The inner domain of the model (where WSA is utilized) is denoted by the central white circle. (c–f) Magnetic field measurements (sampled at a rate of 20 s^{-1}) taken during a CME-driven compressed magnetosphere pass on 23 November 2011 are displayed in MSM coordinates. The locations of the northern cusp, magnetopause (MP), and multiple bow shock (BS) crossings are labeled.

The magnetic field measured by MESSENGER over a 90 min interval beginning on 23 November 2011 is displayed in Figures 4c–4f. The sequence begins with MESSENGER just north of the plasma sheet ($X_{MSM} = -2.4$, $Y_{MSM} = 0.44$, $Z_{MSM} = 0.07$) R_M, and then the spacecraft passed over the northern polar region. After passing through periapsis near Mercury's north pole, MESSENGER headed southward, first traversing a broad magnetospheric cusp within which the total field was highly variable and often depressed by more than 100 nT. The spacecraft then crossed the magnetopause and thereafter experienced multiple crossings of the bow shock. The magnetic field intensity at the magnetopause was 321 nT. Starting just poleward of the cusp and continuing through the high-altitude dayside magnetosphere, the magnetic field exhibited

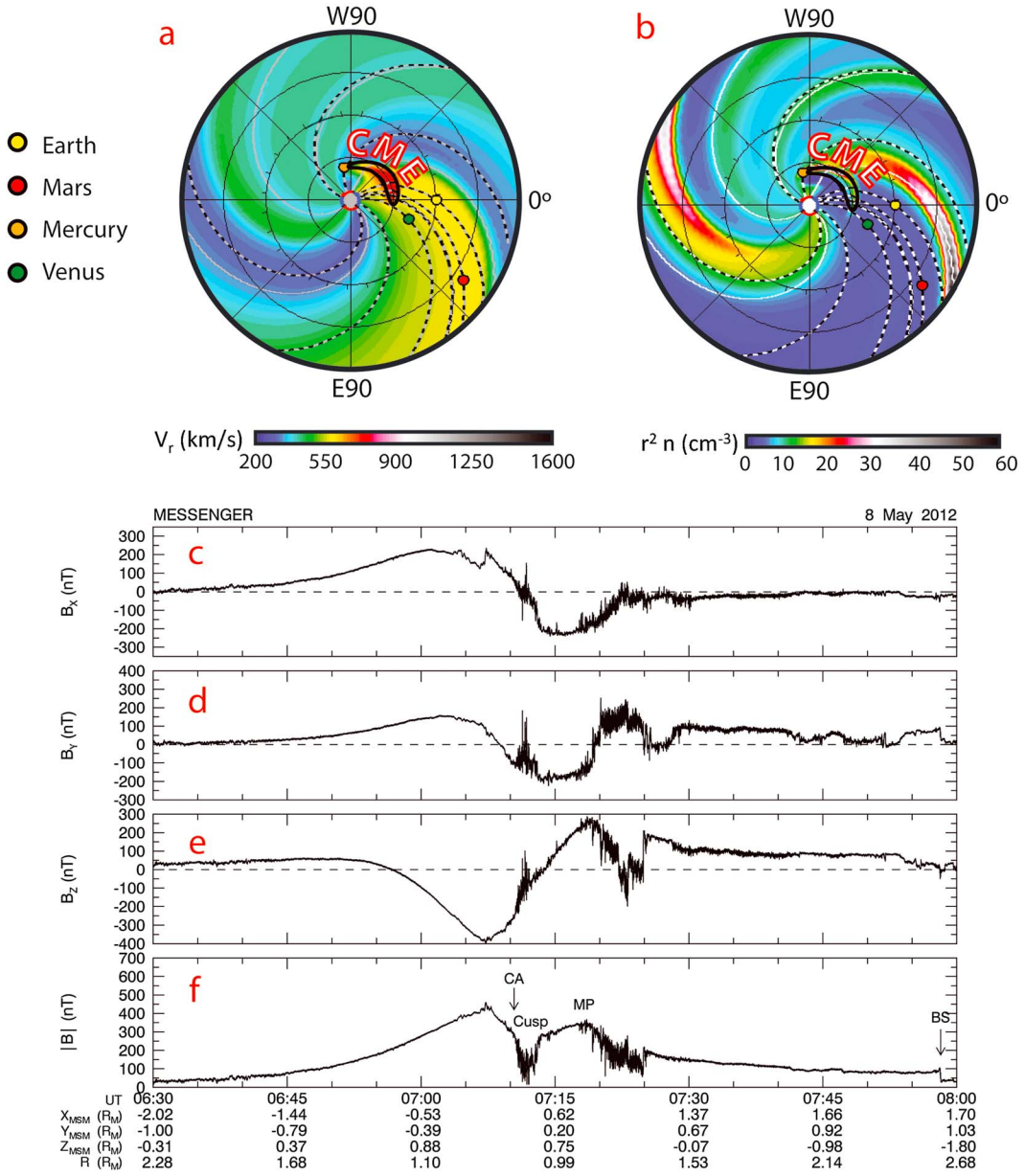

Figure 5. ENLIL-WSA models of (a) solar wind speed and (b) the product of the density and the square of the distance from the Sun in AU on 8 May 2012 at 12:00 UTC. As shown, the edge of a coronal mass ejection passed over Mercury as it moved radially away from the Sun. (c–f) Magnetic field measurements (sampled at a rate of 20 s^{-1}) taken during a CME-compressed magnetosphere pass on 8 May 2012 are displayed in MSM coordinates. The locations of the northern cusp, magnetopause (MP), and bow shock (BS) are labeled.

large-amplitude perturbations in response to a phenomenon we term cusp plasma filaments, as well as flux transfer events, as discussed below. The outward motion of the bow shock appears to have been the result of a decreasing upstream Mach number. The decreasing Mach number is reflected in the declining magnetic field jumps across each succeeding shock crossing. The low upstream Mach number is also reflected in the near-constant magnetic field intensity across the magnetopause, indicative of a strong plasma depletion layer [*Zwan and Wolf*, 1976; *Gershman et al.*, 2013]. Low solar wind Mach number conditions are especially common during CMEs [e.g., *Farrugia et al.*, 1995; *Lavraud and Borovsky*, 2008; *Sarantos and Slavin*, 2009].

The corresponding WSA-ENLIL simulation results for 8 May 2012 at 12:00 UTC are shown in Figure 5. For this event, too, a CME passed over Mercury. However, in this case the simulation indicates that the CME did not

Table 2. Magnetopause Analysis Results

Year	DOY	UTC	X'_{MSM} Y'_{MSM} Z'_{MSM} (R_M)	$\mathbf{B_N}/B_N$	B_N (nT)	Shear Angle (°)	α[a]	β_{MSH}[b]
2011	327	10:21:18	(1.07, −0.14, 0.46)	(0.95, −0.09, 0.30)	31.9	59.6	0.10	0.06
2012	129	07:19:11	(0.83, 0.45, 0.56)	(0.86, 0.31, 0.39)	70.3	27.3	0.22	0.74
2012	132	23:21:07	(1.01, 0.26, 0.50)	(0.93, 0.17, 0.33)	26.1	148	0.082	0.70
2012	132	23:21:14	(1.02, 0.26, 0.49)	(0.93, 0.17, 0.32)	29.4	157	0.096	0.58
2012	132	23:21:20	(1.02, 0.26, 0.48)	(0.93, 0.17, 0.32)	29.4	159	0.096	1.82
2012	132	23:21:25	(1.02, 0.27, 0.48)	(0.93, 0.18, 0.31)	9.7	160	0.033	1.56
2012	132	23:21:32	(1.03, 0.28, 0.48)	(0.93, 0.18, 0.31)	22.5	166	0.077	8.67

[a]Dimensionless reconnection rate $\alpha = B_N/B_{MP}$.
[b]Determined from equation (2).

pass directly over Mercury, but rather the planet encountered its eastern flank. This event is remarkable in that MESSENGER appears to have remained inside of the bow shock from the inbound encounter at ~18:12 UTC during the previous periapsis pass on 7 May until after the following periapsis pass, with extreme pressure and an outbound bow shock encounter at ~07:58 UTC. The mean 20 min average of the IMF upstream of the bow shock was $B_X = -2.01$ nT, $B_Y = 20.1$ nT, $B_Z = -9.50$ nT, and $B = 27.0$ nT (Table 2). The IMF draping pattern in the magnetosheath was stable after a strong field rotation at ~7:25 UTC just upstream of the magnetopause. Figure 5 shows that this CME is predicted to have had a speed near 800 km/s and a density similar to or greater than that for the 23 November 2011 event. The solar wind speed measured by FIPS upstream of the outbound bow shock was only ~500 km/s (Table 1) compared with the forecast 800 km/s. This difference is likely due to Mercury having passed through the flank region of this CME. As we show below, this event had the highest dynamic pressure of the three considered here. The fact that MESSENGER never emerged into the upstream solar wind between the last periapsis pass on 7 May 2012 and the outbound leg of the first periapsis pass on 8 May 2012 indicates that Alfvénic Mach number was extremely low and the bow shock unusually distant.

The magnetic field measurements for the first periapsis pass on 8 May 2012 are displayed in Figure 5. The geometry of this hot season pass was quite similar to that for the 23 November 2011 event (cf. Figure 3). The 90 min interval started with MESSENGER in the plasma sheet on the nightside ($X_{MSM} = -2.0$, $Y_{MSM} = -1.0$, $Z_{MSM} = -0.3$) R_M. As with the previous event, this pass over the northern polar cap showed another very broad, deep magnetic cusp with multiple short, deep magnetic depressions, and a peak field intensity of 328 nT just inside the magnetopause. The bow shock was, as for the other events, weak and located unusually far from the planet [cf. *Winslow et al.*, 2013]. The IMF for this event was extremely disturbed and variable. As with the 23 November 2011 event, the magnetic field decreased only slightly across the magnetopause, indicating a strong PDL but with a slightly higher plasma β in the magnetosheath than for the previous event (see Table 2).

The WSA-ENLIL simulation results for 11 May 2012 at 24:00 UTC displayed in Figure 6 show a different type of solar wind than for the previous two extreme solar wind pressure events. On this occasion Mercury appears to have encountered the inward edge of a corotating interaction region (CIR) caused by the collision between a high-speed stream, moving at ~600 km/s, and a slower solar wind ahead of it. The FIPS measurements upstream of the bow shock for this periapsis pass gave a speed of only ~425 km/s (Table 1), again supporting the WSA-ENLIL simulation, which shows that Mercury encountered only the edge of the CIR. No evidence for an interplanetary shock is present in the magnetic field measurements, consistent with expectations for a CIR in the inner solar system. Moreover, the IMF decreased in strength between MESSENGER's inbound bow shock crossing for this periapsis pass and the outbound bow shock, where the 20 min averaged IMF was $B_X = 13.0$ nT, $B_Y = -9.51$ nT, $B_Z = -0.20$ nT, and $B = 24.6$ nT. Further, the IMF draping pattern in the forward magnetosheath was variable, with several rotations in the field direction. The magnetic field measurements in Figures 6c–6f show that the bow shock was much stronger and closer than for the two events associated with CMEs. The bow shock crossings also exhibited substantial overshoots indicative of high Mach numbers at Mercury [*Masters et al.*, 2013].

The magnetic field measurements displayed in Figures 6c–6f start with MESSENGER moving north to exit the southern lobe of the tail ($X_{MSM} = -2.6$, $Y_{MSM} = -0.5$, $Z_{MSM} = -1.0$) R_M. In contrast to the other two extreme events, this pass over the northern polar cap shows a shallower magnetic cusp. For this event a series of magnetopause crossings was observed as the spacecraft moved away from Mercury toward the south. The

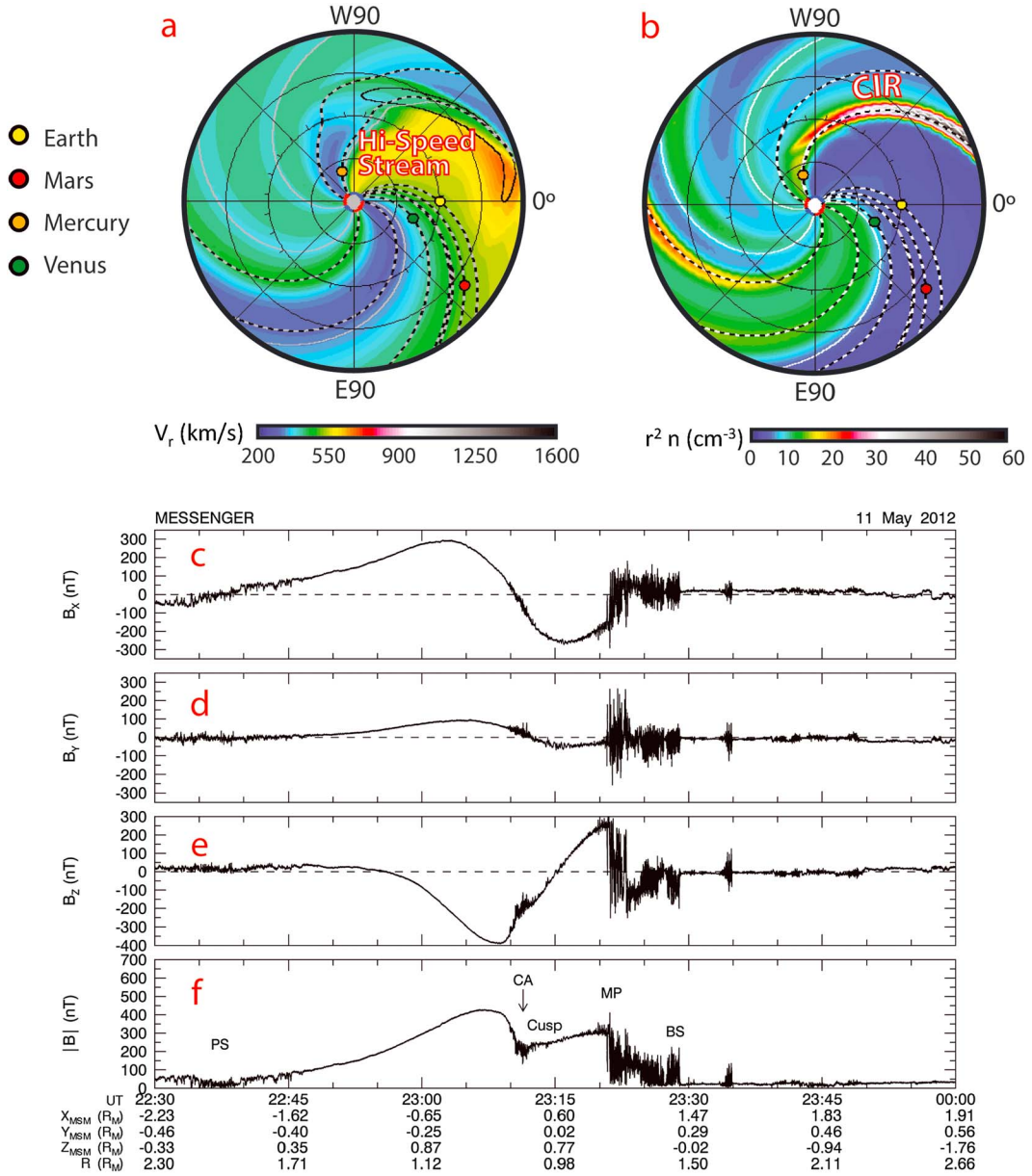

Figure 6. ENLIL-WSA models of (a) solar wind speed and (b) the product of the density and the square of the distance from the Sun in AU on 11 May 2012 at 24:00 UTC. As shown, the edge of a corotating interaction region driven by a high-speed stream passed over Mercury and compressed its magnetosphere. (c–f) Magnetic field measurements (sampled at a rate of 20 s^{-1}) taken during a high-speed stream interval on 11 May 2012 are displayed in MSM coordinates. The locations of the northern cusp, magnetopause (MP), and bow shock (BS) are labeled.

magnetic field intensity just inside the initial magnetopause crossing was 318 nT, and the intensity decreased with each succeeding crossing as would be expected if the underlying cause of the multiple encounters were a slow, continuous decrease in solar wind pressure. As mentioned above, the bow shock was clearly standing in a higher-Mach-number solar wind than the two earlier events, as evidenced by the much thinner magnetosheath and the larger jumps in the magnetic field across the shock. For this event the magnetic field decreased strongly across the magnetopause, and no evident PDL was present. Accordingly, the plasma β in the magnetosheath was much higher than for the 23 November 2011 or 8 May 2012 events. Although some perturbations were present in the magnetospheric magnetic field measurements between the cusp and the magnetopause, the flux transfer event (FTE) signatures were limited to the region around the magnetopause.

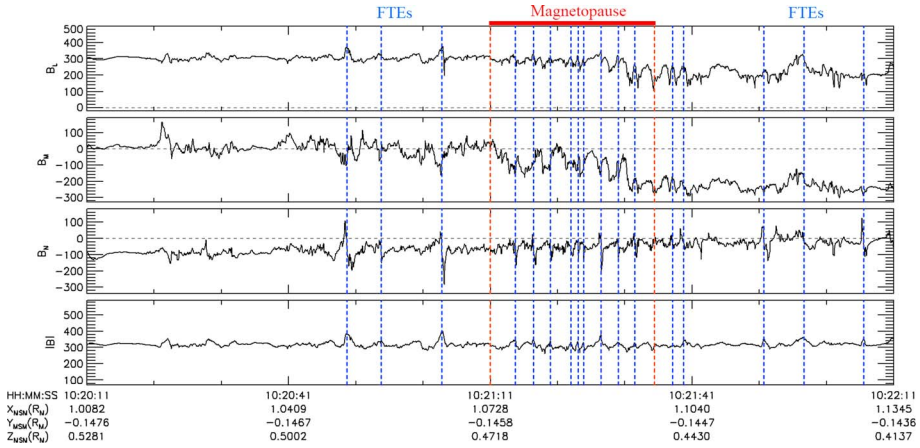

Figure 7. Magnetic field measurements in boundary normal coordinates during a 2 min interval spanning the dayside magnetopause crossing on 23 November 2011. The magnetopause normal adopted for this display was determined from the average magnetopause model of *Winslow et al.* [2013]. Time is in UTC. The start and stop times for magnetic field rotation across the magnetopause current layer are marked by red dashed vertical lines, and the full interval of such rotation is indicated by the horizontal red bar. A number of flux transfer events (FTEs) are indicated by blue dashed vertical lines.

3. Magnetopause Analysis

Minimum variance analysis (MVA) [*Sonnerup and Cahill*, 1967] was performed on each dayside magnetopause crossing during the three extreme solar wind intervals considered here. Large components B_N of the magnetic field normal to the magnetopause were determined for all of the boundary crossings during these events. However, for these extreme intervals the eigenvalue ratios for the magnetopause crossings were marginal (e.g., see discussion of MVA analysis by *DiBraccio et al.* [2013]) because of the presence of large-amplitude fluctuations, particularly those associated with flux transfer events, in the magnetopause current layer. Further, the magnitudes of the magnetic fields normal to the magnetopause determined in this manner were found to be sensitive to the choice of analysis interval, again indicative of high levels of fluctuations and/or rapid temporal variations in orientation of the magnetopause.

For these reasons, we have used the normal vectors to the magnetopause surface determined from the average magnetopause model of *Winslow et al.* [2013]. For their study they adopted the functional form of the *Shue et al.* [1997] model, which has been shown to fit the Earth's magnetopause closely. The magnetopause surface is given by the radial distance from the planetary magnetic dipole

$$\rho = \left(X'_{MSM}{}^2 + Y'_{MSM}{}^2 + Z'_{MSM}{}^2\right)^{0.5} = R_{ss}[2/(1 + \cos\theta)]^{\gamma} \quad (1)$$

where $\theta = \tan^{-1}[(Y'_{MSM}{}^2 + Z'_{MSM}{}^2)^{0.5}/X'_{MSM}]$, R_{ss} is the subsolar standoff distance or the distance from the planetary magnetic dipole to the nose of the magnetopause, and γ is the magnetopause flaring parameter. *Winslow et al.* [2013] found a best fit to three Mercury years of MESSENGER magnetopause crossings for $R_{ss} = 1.45\ R_M$ and $\gamma = 0.5$.

From the normal direction at the point of the magnetopause crossing derived from the *Winslow et al.* [2013] model surface, the magnetic field data in the vicinity of each magnetopause were rotated into the boundary normal coordinates (*L*, *M*, *N*) [*Berchem and Russell*, 1982]. In this coordinate system *N* is normal to the magnetopause, *L* is perpendicular to *N* and lies in the plane defined by *N* and Z_{MSM}, and *M* completes the right-handed system. The magnetic field component normal to the magnetopause for each orbit was computed by averaging the B_N component of the magnetic field across the width of the magnetopause current layer. The magnetic field shear angle, or rotation, across the magnetopause current layer and the reconnection rate, $\alpha = B_N/B_{MP}$, where B_{MP} is the magnitude of the magnetic field immediately inside the magnetopause [*Sonnerup et al.*, 1981; *DiBraccio et al.*, 2013], were also computed and are given in Table 2.

3.1. 23 November 2011

Magnetometer measurements across the dayside magnetopause on 23 November 2011 are displayed in boundary normal coordinates in Figure 7. The normal magnetic field direction derived from the mean

magnetopause model of *Winslow et al.* [2013], in aberrated MSM coordinates, for the outbound magnetopause crossing on 23 November 2011 is $\mathbf{B_N}/B_N = (0.95, -0.09, 0.30)$. The model magnetopause is at an altitude of only 685 km, or 0.28 R_M, as shown in Figure 3. For the first minute of the interval, MESSENGER was inside the magnetosphere, as evidenced by the magnetic field components $B_L \sim +300$ nT and $B_M \sim 0$ nT. The magnetic field in the magnetosheath after exiting the magnetopause current layer satisfied $B_L \sim 200$ nT and $B_M \sim 250$ nT. This magnetopause crossing occurred at a magnetic latitude of 25.4° and just slightly prenoon (Figure 3). The magnetic shear angle θ was calculated to be 59.6°. The normal component to the magnetopause was strongly negative at the beginning of the 2 min interval, reflecting the inward orientation of the planetary dipole magnetic field at low altitude in the northern hemisphere. The direction of the normal component of the magnetic field beyond the magnetopause was small and slightly positive, reflecting the field draping in the magnetosheath and the average IMF direction (Table 1). The B_N component transitioned from primarily inward (negative) to outward (positive) near the outer edge of the current layer as expected for a stable rotational discontinuity northward of an extended low-latitude X line [e.g., *Paschmann et al.*, 2013]. Averaged over the full width of the current sheet, $B_N = -31.9$ nT and the dimensionless reconnection rate, B_N/B_{MP}, was 0.10, which is typical of the values reported earlier for MESSENGER magnetopause crossings [*Slavin et al.*, 2009; *DiBraccio et al.*, 2013]. For Earth and Mercury the mean dimensionless reconnection rate values are ~0.05 [*Mozer and Retinò*, 2007] and 0.15 [*DiBraccio et al.*, 2013], respectively. Uncertainties in the normal magnetic field component and the reconnection rate are difficult to estimate, but they are likely to be in the ~10–30% range [*DiBraccio et al.*, 2013]. Hence, the reconnection rate for this magnetopause is high relative to the mean for Earth, but somewhat less than the average at Mercury.

Following the methodology of *DiBraccio et al.* [2013], we assume pressure balance and calculate the ratio of thermal to magnetic pressure in the magnetosheath, β_{MSH}, from the magnetic field intensities just inside the magnetopause, B_{MP}, and in the adjacent magnetosheath, B_{MSH}:

$$\beta_{MSH} = (B_{MP}/B_{MSH})^2 - 1 \tag{2}$$

yielding $\beta_{MSH} = 0.06$. We confirmed the assumption of negligible plasma pressure just inside the magnetopause by using the magnetosheath thermal pressure estimated from FIPS data (see below) to determine that β_{MSH} is of order 10^{-2}.

Under the assumption that the magnetic pressure dominates the plasma pressure just inside the magnetopause, which appears justified on the basis of FIPS measurements [*DiBraccio et al.*, 2013], the subsolar point and the solar wind ram pressure, P_{sw}, may be inferred from Newtonian pressure balance [*Spreiter et al.*, 1966] by taking into account the angle ψ between the magnetopause normal and the solar wind direction (assumed to be radial in aberrated MSM coordinates):

$$P_{sw} = \left(B_{MP}{}^2/2\mu_o\right)/\left(0.88 \ \cos^2 \ \psi\right) \tag{3}$$

where μ_o is the magnetic permeability of free space. The magnetic field magnitude inside the magnetopause was observed to be B_{MP} ~319 nT, and for an angle of incidence $\psi = 18.5°$, the dynamic pressure of the upstream solar wind was 51.0 nPa (Tables 1 and 2).

Just upstream of the bow shock on 23 November 2011, FIPS measurements indicated a solar wind speed of ~450 km/s, but solar wind density n cannot be directly determined [*Gershman et al.*, 2013]. However, in the subsonic region just planetward of the bow shock, FIPS measurements indicate that $n_p \sim 350$ cm^{-3} and the plasma temperature was $T_p \sim 2.5$ MK. Given the factor of 2.5 jump in magnetic field intensity and, therefore, plasma density across this quasi-perpendicular bow shock, we estimate that upstream solar wind density was ~140 cm^{-3}. Combined with the direct measurement of solar wind speed, the upstream M_A was ~2.5, and the solar wind dynamic pressure was ~47 nPa. The calculated solar wind dynamic pressure matches well the magnetic pressure measured inside the near-subsolar magnetopause, supporting the robustness of the technique and the assumption that plasma pressure just inside of the magnetopause may be neglected. The low upstream M_A value and quasi-perpendicular shock geometry produced a large-scale plasma depletion layer, resulting in the low value of β at the magnetopause [*Gershman et al.*, 2013]. Such large-scale flux pileup has been observed at Earth for CME events with low upstream M_A [*Farrugia et al.*, 1995].

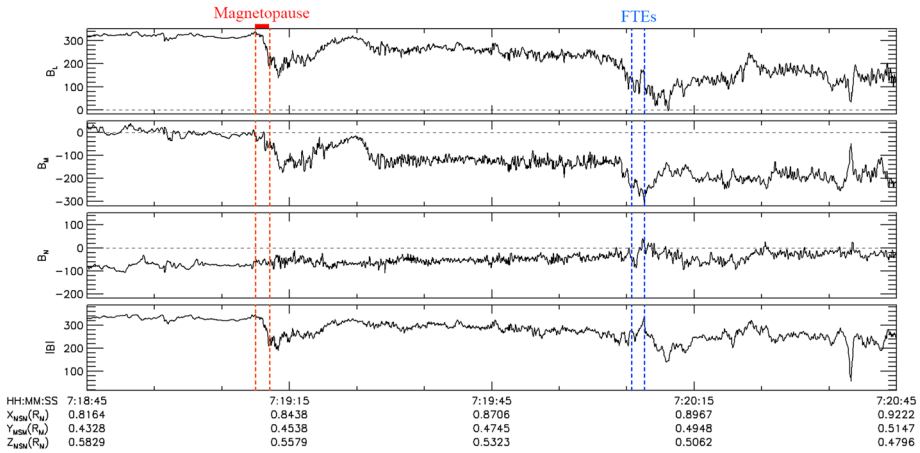

Figure 8. Magnetic field measurements in boundary normal coordinates during a 2 min interval spanning the dayside magnetopause crossing on 8 May 2012. The magnetopause normal adopted for this plot was determined from the average magnetopause of *Winslow et al.* [2013]. See Figure 7 for other information.

3.2. 8 May 2012

Magnetometer measurements across the magnetopause on 8 May 2012 are displayed in boundary normal coordinates in Figure 8. The normal magnetic field direction for the outbound magnetopause crossing, derived from the mean magnetopause model of *Winslow et al.* [2013] and in aberrated MSM coordinates, was $\mathbf{B_N}/B_N = (0.86, 0.31, 0.39)$. The model magnetopause is at an altitude of only 535 km and magnetic latitude of 26.7°, as shown in Figure 3. However, this traversal of the magnetosphere-magnetosheath interface showed notable similarities to the "double magnetopause" observed during the first MESSENGER flyby of Mercury [*Slavin et al.*, 2008]. As described by *Slavin et al.* [2008] and in greater detail by *Anderson et al.* [2011b] and *Raines et al.* [2011], the complete transition from magnetosphere to magnetosheath during the first flyby took the form of two current sheets separated by a boundary layer region. For the first minute of the interval in Figure 8, MESSENGER was inside the magnetosphere, as evidenced by the magnetic field components $B_L \sim +320$ nT and $B_M \sim 0$ nT. The magnetic field in the boundary layer region, which ended with a second magnetopause-like rotation in the magnetic field and the observation of two FTEs at ~07:20:04:10 UTC, was intermediate in both magnitude and the level of fluctuations between what was measured planetward of the inner current sheet and sunward of the second, outermost current sheet. In the magnetosheath upstream of this second magnetopause-like current we observed (see Figure 8) $B_L \sim 100$ nT and $B_M \sim 160$ nT. The normal magnetic field component, B_N, had a mean value of -70.3 nT across the inner magnetopause current layer, became steadily less negative across the boundary layer, and then fluctuated about zero upstream of the second magnetopause. The magnetic shear angle was only 27.3°. The dimensionless reconnection rate, B_N/B_{MP}, was therefore 0.22, which is the largest value for the magnetopause crossings examined in this study. It is also greater than the mean of ~0.15 found by analysis of a large number of Mercury magnetopause crossings [*DiBraccio et al.*, 2013]. The method for calculating magnetosheath β of *DiBraccio et al.* [2013] results in $\beta_{MSH} \sim 0.74$. This low value is consistent with a value of $\beta_{MSH} \sim 0.5$ calculated from the FIPS and MAG measurements. The magnetic field magnitude inside the magnetopause was observed to be B_{MP} ~328 nT. Following the same approach as for the 23 November 2011 event, the solar wind dynamic pressure inferred from our magnetopause analysis is 61 nPa (Table 1).

3.3. 11 May 2012

During the 11 May 2012 high-speed stream event, the MESSENGER observations contain at least five distinct magnetopause crossings, as well as other partial, less clear encounters both slightly before and slightly after this interval, as shown in Figure 9. The first magnetopause crossing occurred at 23:21:07 UTC at a magnetic latitude of 26.4° and an altitude of 615 km, as shown in Figure 3. Four additional full magnetopause crossings occurred over the next ~30 s, at altitudes up to ~640 km. There were a large number of FTEs during the crossing, but unlike the situation for the 23 November 2011 event, the FTEs on 11 May were all confined to the vicinity of the magnetopause encounters. The mean time

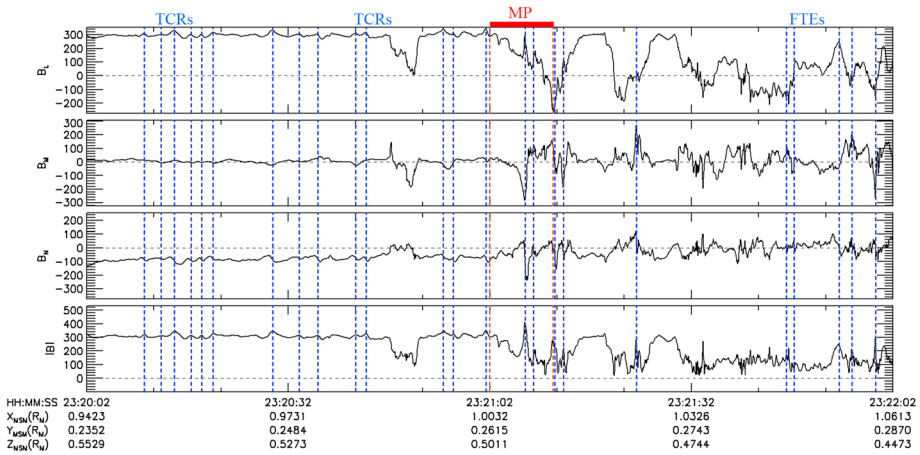

Figure 9. Magnetic field measurements in boundary normal coordinates during a 2 min interval spanning the dayside magnetopause crossing on 11 May 2012. The magnetopause normal adopted for this plot was determined from the average magnetopause of *Winslow et al.* [2013]. See Figure 7 for other information.

between the FTEs was ~4 s, and many good examples of FTE-type flux ropes were present, such as the large-amplitude FTE observed in the magnetopause current layer at 23:21:32 UTC. In addition to the FTEs for which MESSENGER penetrated the structure and observed the characteristic helical magnetic field pattern, there were also many FTE-type traveling compression regions (TCRs) in the magnetic field measurements. These TCR signatures are produced when FTE-type flux ropes are pushed against the magnetopause and compress the internal magnetic field as the solar wind drags them downstream [e.g., *Zhang et al.*, 2008; *Slavin et al.*, 2012a].

The IMF in the magnetosheath on 11 May 2012 was variable, but it always displayed a southward component. The magnetic shear angle rotations across these magnetopause crossings were all large and varied from 148 to 166°. The aberrated model normal for the first magnetopause crossing was $\mathbf{B_N}/B_N = (0.93, 0.17, 0.33)$. A negative B_L was observed after this innermost magnetopause crossing and each to follow, whereas B_M was near zero throughout the interval shown in Figure 9. The normal component, B_N, transitioned from positive to negative across each of the magnetopause crossings, with an average normal field magnitude across the innermost magnetopause current layer of − 26.1 nT. For the magnetopause current layers encountered later, the normal magnetic field components ranged from − 9.7 to − 29.4 nT (Table 2). The dimensionless reconnection rate resulting from this first magnetopause crossing was B_N/B_{MP} ~0.08, and the range for the later crossings was 0.03 to 0.1 with a mean of 0.08.

These reconnection rates are about half of the average rate determined by *Slavin et al.* [2009] and *DiBraccio et al.* [2013], and they are the lowest reconnection rates inferred for the three extreme events considered in this study. These low rates were measured during intervals of strongly southward IMF and large magnetic shear angles across the magnetopause. The reason for the low reconnection rates compared with those during the 23 November 2011 and 8 May 2012 events appears to be the generally high magnetosheath plasma β values, inferred from the magnetic field, of up to 8.7 for these magnetopause crossings (Table 2). An inverse correlation between reconnection rate and magnetosheath β has been documented at Earth [*Scurry et al.*, 1994; *Anderson et al.*, 1997; *Phan et al.*, 2013] and was recently found for Mercury [*DiBraccio et al.*, 2013]. The low reconnection rate and high-β magnetosheath found during this high-speed stream event stands in contrast with the two CME events with their higher reconnection rates and low-β magnetosheaths.

The magnetic field intensities just inside the magnetopause during these crossings ranged from 318 nT for the first full crossing to 292 nT for the last. On the basis of the estimation technique applied to the 23 November 2011 and 8 May 2012 events, the solar wind dynamic pressure inferred during the first magnetopause crossing on 11 May was 53 nPa. The solar wind dynamic pressure decreased for each succeeding magnetopause crossing until a value of 44.3 nPa was reached for the fifth and final complete crossing (Table 2), consistent with an outward expansion of the magnetopause that overtook MESSENGER multiple times as it moved away from the planet.

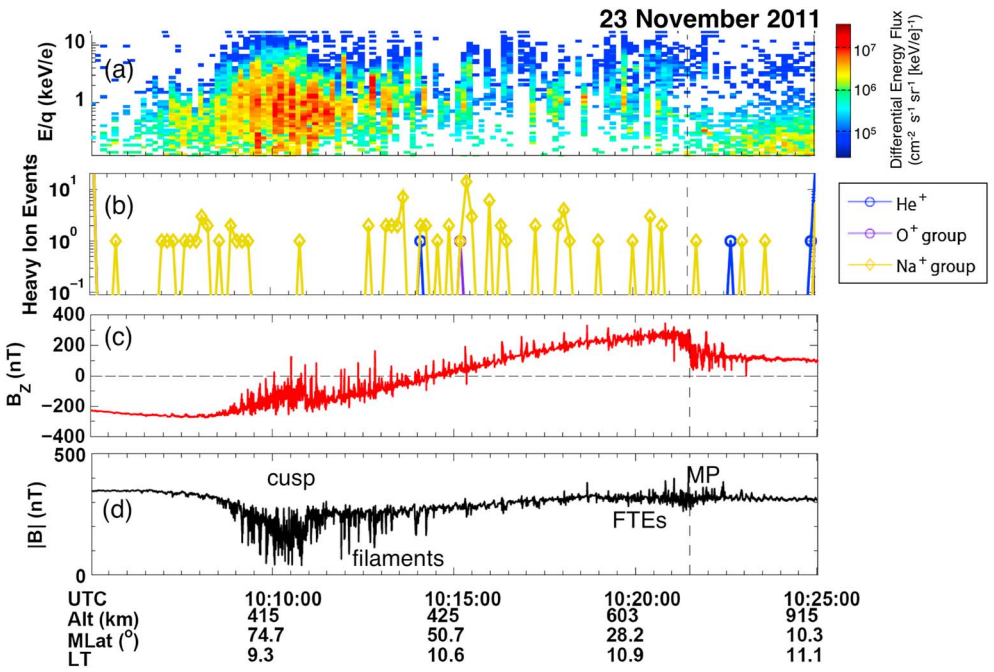

Figure 10. (a) Proton differential energy flux versus energy per charge (E/q) and time during the periapsis pass of 23 November 2011. (b) Heavy ion counts binned by three composition types; He^+, O^+ group ($m/q = 14–20$), and Na^+ group ($m/q = 21–30$). (c) B_Z in MSM coordinates and (d) total magnetic field intensity versus time. The locations of the cusp and magnetopause (MP) are labeled, as are times when FTEs and cusp plasma filaments were observed. MLat, ALT, and LT denote magnetic latitude, altitude, and local time, respectively.

4. Northern Cusp Observations

Winslow et al. [2012] conducted the first investigation of Mercury's northern magnetospheric cusp. They found that the mean extent of the cusp is 4.5 h in local time and 11° in magnetic latitude. The equatorward boundary of the cusp is defined as the locus of the most poleward closed field lines in the forward magnetosphere. As reconnection changes the relative amounts of closed and open magnetic flux in the low- and high-latitude magnetosphere, respectively, the cusp is expected to move in latitude. At Earth the cusp moves equatorward (poleward) with southward (northward) IMF [*Burch*, 1973; *Zhou and Russell*, 1997]. The range of latitude over which *Winslow et al.* [2012] found the cusp to be encountered by MESSENGER was ~28°, but no clear correlation with IMF B_Z could be found. However, they did find that the depth of the diamagnetic decrease in the northern cusp magnetic field increases with negative IMF B_X and increasing solar wind ram pressure. Negative B_X is expected and has been observed to produce strong reconnection at the anti-sunward boundary of Mercury's northern cusp, on the basis of a variety of evidence including "FTE showers" [*Slavin et al.*, 2012a]. Although this type of reconnection does not affect the balance between closed and open magnetic flux, it does inject solar wind plasma directly into the cusp and enhances the diamagnetic decrease. Here we examine the northern cusp in the MAG and FIPS measurements that were taken during the three extreme solar wind passes identified in this study. From Figure 3 it can be seen that these periapsis passes all lie within the region where *Winslow et al.* [2012] most frequently observed the cusp.

4.1. 23 November 2011

MAG and FIPS measurements collected during MESSENGER's crossing of the northern cusp on 23 November 2011 are displayed in Figure 10. As observed by *Winslow et al.* [2012], the poleward boundary of the cusp is marked by enhanced fluctuations and a general decrease in the magnetic field intensity beginning at approximately 10:08:40 UTC and magnetic latitude 80.3°. The minimum in the long-wavelength magnetic field strength in the cusp was ~150 nT at ~10:10:30 UTC and magnetic latitude 72.7°. However, the cusp is seen here to have been composed of narrow, few-seconds-long intervals during which the field strength was reduced to values as low as ~50 nT. The long-wavelength magnetic field recovered to ~250 nT by 10:11:00 UTC

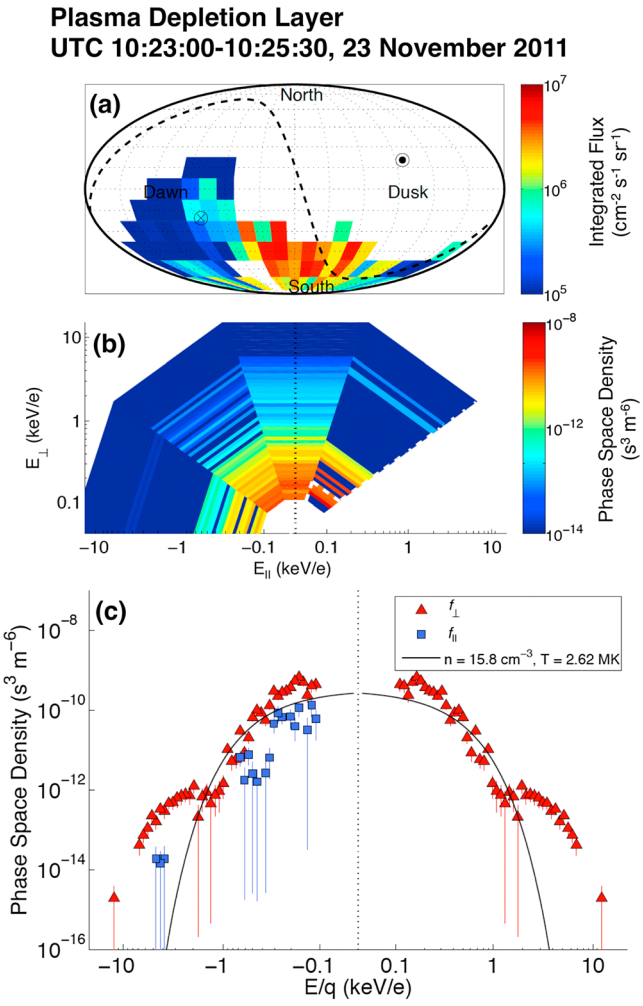

Figure 11. (a) All-sky map of integrated proton flux in the plasma depletion layer on 23 November 2011. Ion fluxes are transformed into 15° angular bins in MSO coordinates and integrated from 100 eV/*e* to 13.7 keV/*e*. The circle with the dot, circle with the cross, and dashed lines correspond to particles with 0°, 180°, and 90° pitch angles, respectively. A detailed description of the construction of all-sky maps and distribution functions from FIPS three-dimensional data has been provided by *Raines et al.* [2014] and *Gershman et al.* [2014]. The north and south poles and the dawn and dusk directions are indicated. (b) Proton phase space distribution; the vertical axis is particle energy perpendicular to the local magnetic field and the horizontal axis is particle energy parallel (positive values) and antiparallel (negative values) to the magnetic field. (c) The proton distribution function parallel, $f_{||}$, and perpendicular, $f_\perp$, to the magnetic field are displayed and fit to determine temperature.

with MESSENGER at 70.3° magnetic latitude. But, the narrow discrete decreases in magnetic field intensity, which began poleward of the cusp proper and exceeded 100 nT in depth, continued until 10:14:15 UTC and 54.3° magnetic latitude. This point is more than 15° farther equatorward than where the large-scale decrease in the cusp magnetic field ended.

We call these several-second-long discrete diamagnetic decreases "cusp plasma filaments," reflecting their spatial association with the cusp. We use the term filament to reflect the presumed diamagnetic origin of the field decrease, implying columns of enhanced plasma density aligned with the local magnetic field. The total latitudinal extent of the cusp crossing on 23 November 2011, on the basis of the large-scale magnetic field decrease, was ~10°, and the maximum diamagnetic decrease was ~200 nT, or 16 nPa of equivalent plasma pressure. These values compare with the typical cusp values of ~11° and thermal plasma pressures of 2 to 3 nPa [*Winslow et al.*, 2012]. This comparison suggests that the major differences between this extreme solar wind pressure event and the more typical cusp is the greater depth of the diamagnetic decrease and the presence of these isolated cusp filaments that began poleward of the cusp and extended to latitudes at least as low as 54° magnetic latitude. Below this latitude the fluctuations in the magnetic field continued, but they corresponded to flux transfer events. In the next section both the cusp filaments and the FTEs observed during this event are further examined.

FIPS proton differential energy flux measured during this periapsis pass is displayed in Figure 10a. Consistent with the earlier surveys of the FIPS plasma data [*Zurbuchen et al.*, 2008; *Raines et al.*, 2014], high fluxes of protons with energies from ~100 eV to ~3 keV were measured during the cusp pass. Na^+-group ions, defined to be ions with mass per charge $m/q = 21–30$ [*Raines et al.*, 2013] (Figure 10b), were observed at a moderately constant count rate across the full periapsis pass. Short-lived enhancements in the proton flux near 1 keV were observed from the poleward edge of the cusp all the way down to the magnetopause at ~25.4° magnetic latitude. We show below that at higher latitudes these single-energy-scan proton flux enhancements were

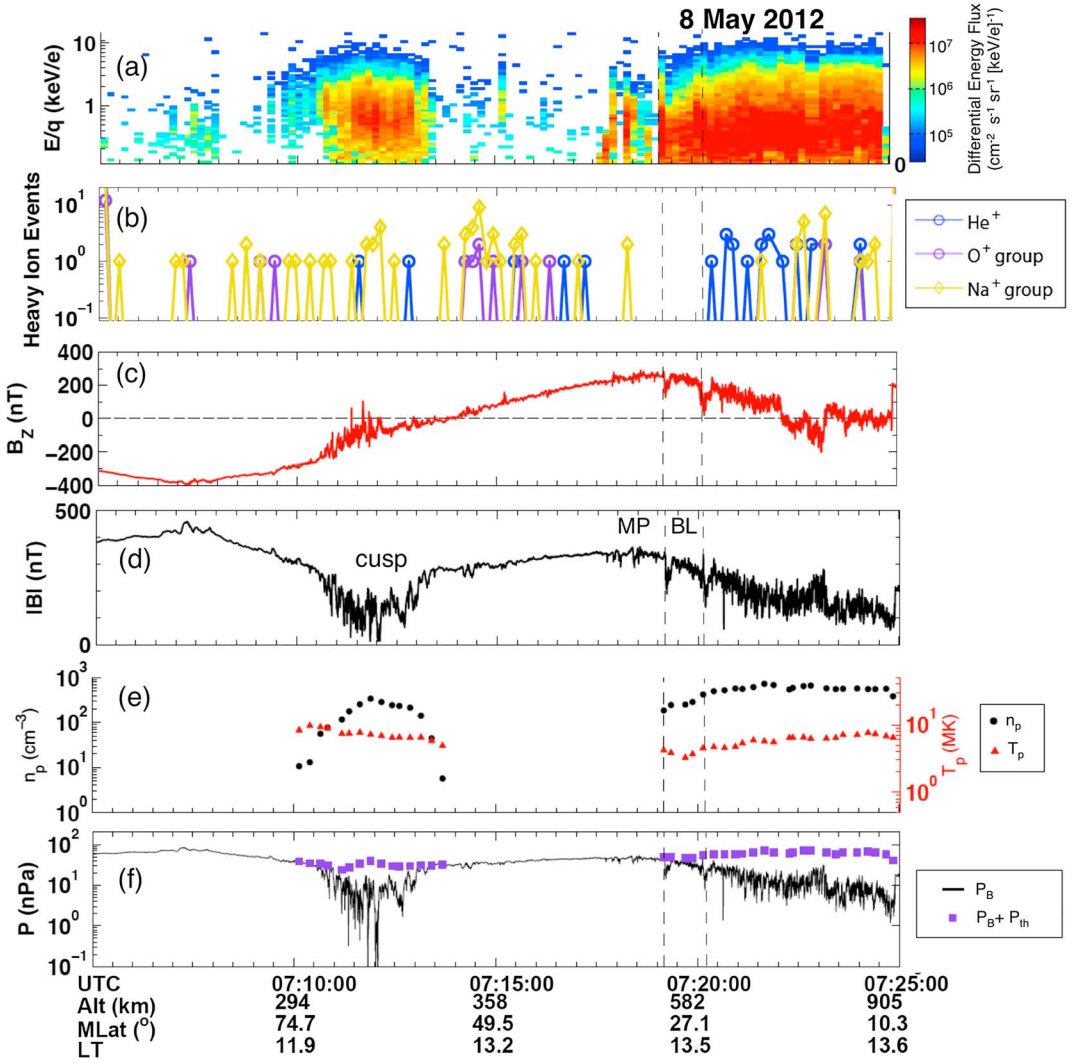

Figure 12. (a) Proton differential energy flux versus energy per charge and time for the periapsis pass of 8 May 2012. (b) Heavy ion counts binned by He^+, O^+ group, and Na^+ group. (c) B_Z in MSM coordinates, (d) total magnetic field intensity, (e) proton density (black circles) and temperature (red triangles), and (f) magnetic pressure P_B and the sum of P_B and proton thermal pressure P_{th}. The locations of the cusp region and the two magnetopause crossings are shown.

generally correlated with the narrow cusp filaments, whereas at lower latitudes these peaks in the proton flux were frequently coincident with FTE signatures in the magnetic field data.

The near-constant magnetic field intensity across the magnetopause on 23 November 2011 indicates that a strong plasma depletion layer was present in the adjacent magnetosheath. Figure 11 presents the FIPS proton measurements just upstream of the magnetopause between 10:23:00 and 10:25:30 UTC. The field of view available to FIPS was limited, as shown in Figure 11a. Hence, under the assumption of gyrotropy, most of the distribution function can be imaged as displayed (Figure 11b). Moment-based calculations of density and a single isotropic temperature yield values of 15.8 cm^{-3} and 2.62 MK (Figure 11c). When distinct temperatures parallel and perpendicular to the local magnetic field vector are allowed, the resulting values are $T_{\|} = 1 \times 10^6$ K and $T_{\perp} = 3 \times 10^6$ K, respectively, consistent with the expected perpendicular heating in the PDL as a result of compression by the pressure of the upstream solar wind [*Zwan and Wolf*, 1976; *Gershman et al.*, 2013]. Given the ~315 nT magnetic field magnitude, the plasma β in the PDL given a single isotropic temperature is only 2×10^{-3}, consistent with the lack of any change in magnetic field magnitude across the magnetopause.

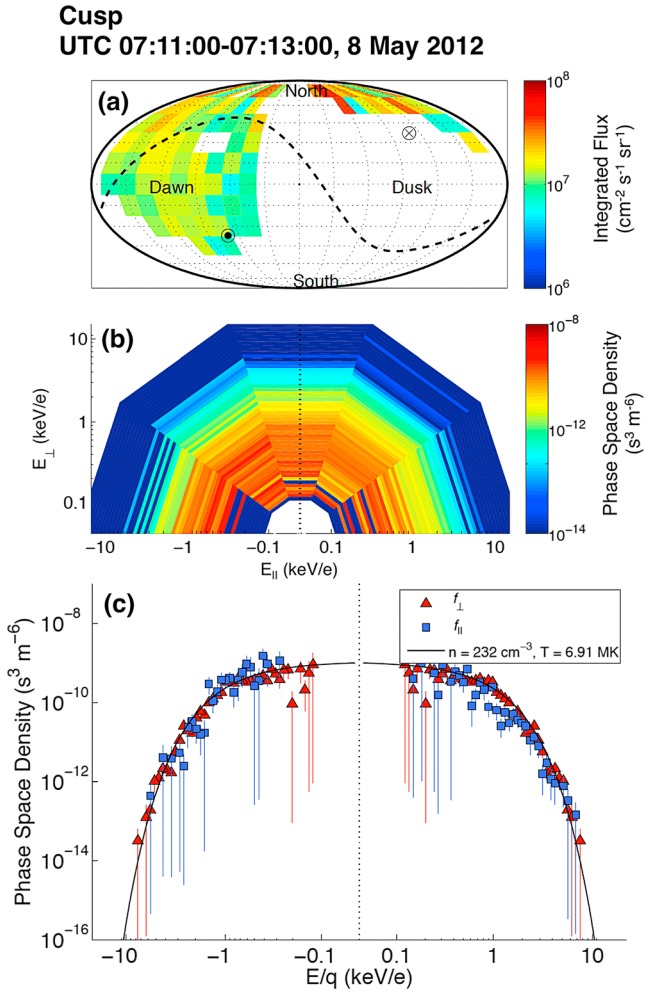

Figure 13. (a) All-sky map of integrated proton flux in the northern cusp on 8 May 2012. Ion fluxes are transformed into 15° angular bins in MSO coordinates and integrated from 100 eV/*e* to 13.7 keV/*e*. The circle with the dot, circle with the cross, and dashed lines correspond to particles with 0°,180°, and 90° pitch angles, respectively. A detailed description of the construction of all-sky maps and distribution functions from FIPS three-dimensional data has been provided by *Raines et al.* [2014] and *Gershman et al.* [2014]. The north and south poles and the dawn and dusk directions are indicated. (b) Proton phase space distribution. (c) Fit of a single temperature to the proton distribution function parallel, $f_{||}$, and perpendicular, $f_\perp$, to the magnetic field.

4.2. 8 May 2012

MAG and FIPS measurements for the outbound passage on 8 May 2012 from the poleward side of the cusp through the dayside subsolar magnetopause crossing are shown in Figure 12. The FIPS measurements for 8 May are similar in many respects to those for 23 November 2011. The planetary ions were present from poleward of the cusp through the magnetopause at magnetic latitude ~ 26.7°. However, from the proton data it is clear that the field of view was much more favorable than for the earlier extreme event, and the overall flux levels were substantially higher. The high-latitude boundary of the cusp, on the basis of the onset of the large diamagnetic decrease in the total magnetic field intensity, occurred at 07:10:50 UTC when MESSENGER was at 70.5° magnetic latitude. The center of the large-scale diamagnetic decrease was at ~ 07:12:00 UTC, which corresponds to 64.7° magnetic latitude. Short-duration diamagnetic decreases in the cusp magnetic field intensity were present, as during the 23 November 2011 event, but they were somewhat deeper and reached minimum magnetic field intensities of less than 20 nT. The equatorward edge of the cusp in the large-scale diamagnetic signature on 8 May 2012 was at ~ 07:13:00 UTC and occurred at a magnetic latitude of ~ 57.9°. Unlike the cusp passage on 23 November 2011, there were no further deep diamagnetic decreases south of the equatorward edge of the main diamagnetic decrease, and the FTE activity was limited to the region immediately adjacent to the magnetopause. Close inspection of the proton spectra in Figure 12a also shows the clear signature of the boundary layer between the two magnetopause-like magnetic field rotations, as discussed earlier.

The proton density and temperature can be determined for individual FIPS energy scans because of the higher overall flux in this cusp; these quantities are displayed in Figure 12e. In the cusp region the correlation between the hot, dense proton population and the large-scale diamagnetic decrease in the total magnetic field is clear, as expected from previous studies [*Winslow et al.*, 2012; *Raines et al.*, 2014]. In the magnetosheath, the density and temperature increase away from the magnetopause toward the bow shock in a manner consistent with a plasma depletion layer [*Gershman et al.*, 2013], albeit not as depleted as was seen on 23 November 2011, when no change in magnetic field intensity was evident across the magnetopause. Figure 12f shows that the proton densities and temperatures determined from the FIPS

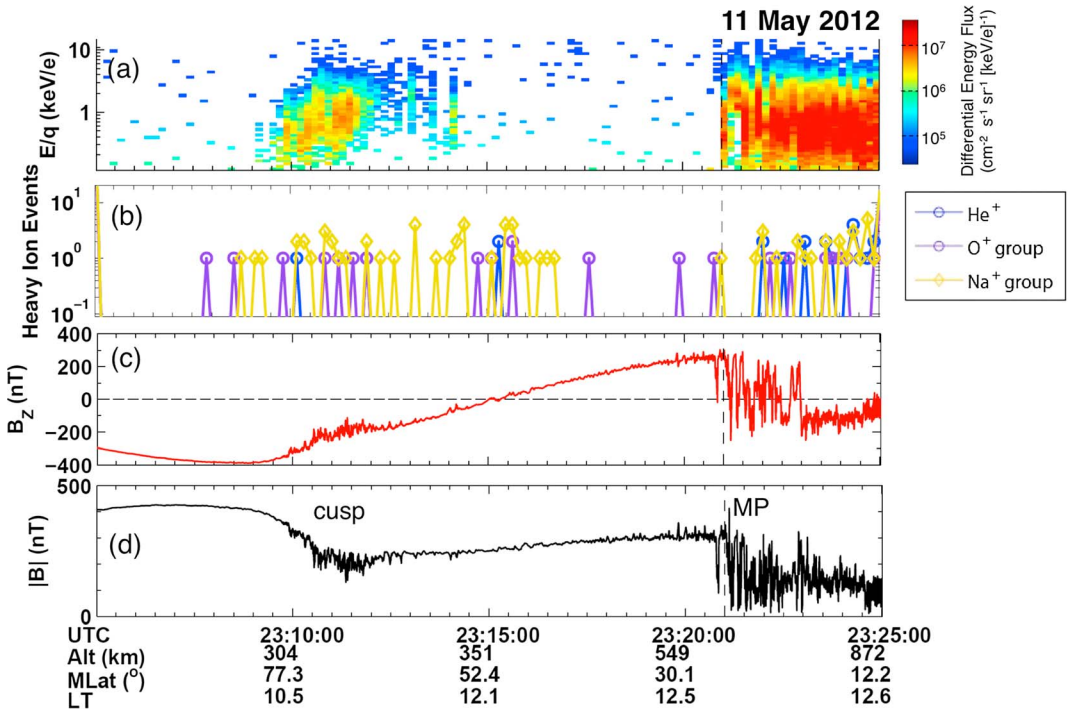

Figure 14. (a) Proton differential energy flux versus energy per charge and time for the periapsis pass of 11 May 2012. (b) Heavy ion counts binned by He^+, O^+ group, and Na^+ group. (c) B_Z in MSM coordinates. (d) Total magnetic field intensity. The locations of the cusp and magnetopause are shown.

measurements produced thermal pressures that match the diamagnetic decreases in the cusp and bring the magnetic and plasma pressures across the magnetopause into approximate balance.

The proton distribution integrated over the cusp interval along with the field of view and moment-derived equivalent Maxwellian distribution for the cusp data [*Gershman et al.*, 2013; *Raines et al.*, 2014] are shown in Figure 13. The distribution function is clearly much more isotropic than for the 23 November 2011 event, as evidenced by comparing the various angular bins in Figure 13b. The parallel and perpendicular slices of the distribution function also agree well with the modeled Maxwellian (black line). Taking moments of this distribution, summed over the entire cusp, yields $n_p = 232\,\mathrm{cm}^{-3}$ and $T_p = 6.9$ MK.

4.3. 11 May 2012

MAG and FIPS measurements from the poleward side of the cusp through the dayside subsolar magnetopause crossing for 11 May 2012 are shown in Figure 14. The high-latitude boundary of the cusp, on the basis of the onset of the large-scale diamagnetic decrease in the total magnetic field intensity, occurred at 23:09:54 UTC when MESSENGER was at 77.8° magnetic latitude. The center of the large-scale diamagnetic decrease was at 23:11:08 UTC, a magnetic latitude of 71.9°, and an altitude of 300 km. The diamagnetic decreases in the total cusp magnetic field intensity were less structured than for the 23 November 2011 and 8 May 2012 events, and the overall decrease in the magnetic field intensities was less; the magnetic field did not fall below 150 nT except for two short excursions to ~120 nT. The equatorward edge of the cusp in the diamagnetic signature was at 23:12:47 UTC and a magnetic latitude of ~63.7°. Unlike the cusp crossing during the 23 November 2011 event, there were only two further weak diamagnetic decreases south of the equatorward edge of the main diamagnetic decrease. Also, in contrast with the 23 November 2011 event, but like the 8 May 2012 event, FTE activity was limited to the region adjacent to the magnetopause.

The FIPS proton differential energy flux spectra are shown in Figure 14a. The FOV and look directions for this pass, like those of 8 May 2012, were favorable, and hot proton distributions with energies up to ~1–2 keV were present in the cusp and the magnetosheath adjacent to the magnetopause. Planetary Na^+ and O^+ group ions were present during the pass, but they were primarily closer to the cusp and in the

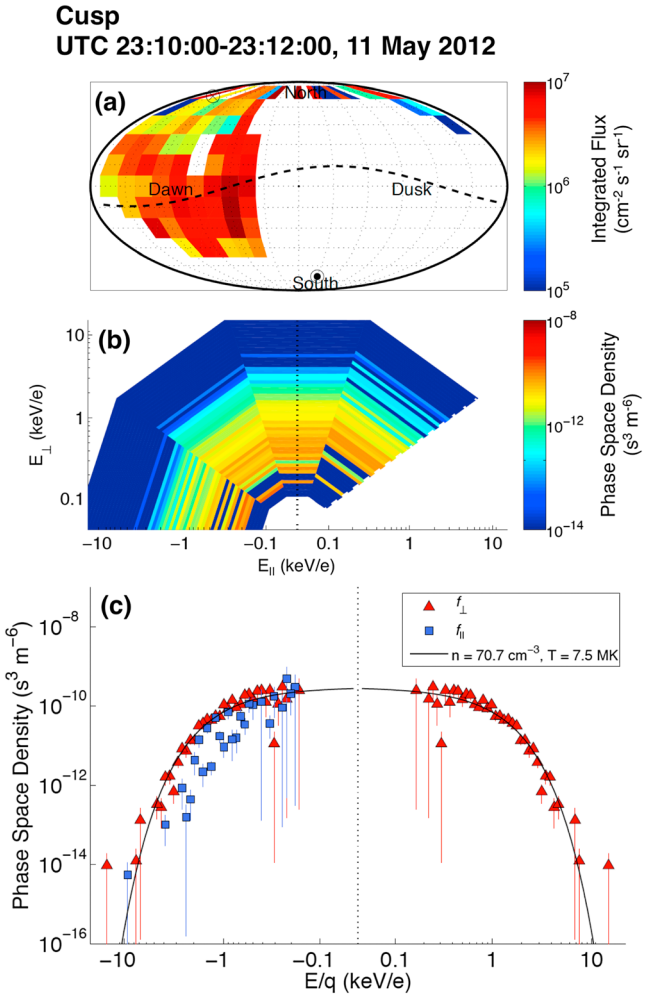

Figure 15. (a) All-sky map of integrated proton flux in the northern cusp on 11 May 2012. Ion fluxes are transformed into 15° angular bins in MSO coordinates and integrated from 100 eV/*e* to 13.7 keV/*e*. The circle with the dot, circle with the cross, and dashed lines correspond to particles with 0°, 180°, and 90° pitch angles, respectively. A detailed description of the construction of all-sky maps and distribution functions from FIPS three-dimensional data has been provided by *Raines et al.* [2014] and *Gershman et al.* [2014]. The north and south poles and the dawn and dusk directions are indicated. (b) Proton phase space distribution. (c) Fit of a single temperature to the proton distribution function parallel, $f_{||}$, and perpendicular, $f_\perp$, to the magnetic field.

magnetosheath. The proton distribution function and Maxwellian fits to the data are intercompared in Figure 15. As shown, the fits to the integrated proton distribution yield $n_p = 70.7\ \mathrm{cm}^{-3}$ and $T_p = 7.5$ MK. Two-dimensional fits for the temperature give $T_{||} = 4$ MK and $T_\perp = 7$ MK, consistent with the apparent anisotropy in the distribution (Figures 15b–15c). Although these proton temperatures are similar, the density is only ~ 30% of that during the 8 May 2012 cusp crossing.

5. Cusp Plasma Filaments and Flux Transfer Events

Cusp plasma filaments recorded just after and equatorward of the magnetospheric cusp encounter on 23 November 2011 are shown in Figure 16. The proton differential energy spectrum for each integration period is displayed in Figure 16a. Because FIPS steps through energy per charge (*E/q*) levels sequentially, from 13.3 keV to 46 eV, with ~150 ms between steps, an alternative display is to distinguish the times of the individual *E/q* steps, as shown in Figure 16b. The cusp filaments can be identified by the brief decreases in field magnitude (Figure 16b). Because each cusp plasma filament was only ~ 1–2 s in duration, the individual 8 s cycle for the measurement of the energy spectra in Figure 16a shows peak differential flux only at the *E/q* step that was being measured at the time that the filament swept over MESSENGER. However, it is clear that strong increases in proton flux were observed whenever FIPS was making measurements for protons near 1 keV, which is close to their mean energy in the magnetosheath, during traversals of these cusp filaments. Lower fluxes were observed when FIPS was making measurements at higher or lower energies as the filament moved over MESSENGER.

Flux transfer events during a comparable interval of MAG and FIPS measurements taken as MESSENGER approached the magnetopause on 23 November 2011 are shown in Figure 17 in the same format as for Figure 16. The FTEs can be identified by the bipolar variations in B_Z that correlate with peaks in the total field. As discussed above (Figure 7), these FTE perturbations record the motion of flux ropes formed at the magnetopause by pulses of reconnection at multiple X lines [*Russell and Elphic*, 1978; *Rijnbeek et al.*, 1984; *Lee and Fu*, 1985, *Wang et al.*, 2005; *Hasegawa et al.*, 2006, 2009]. Strong increases in proton flux were observed whenever FIPS was making measurements near 1 keV for protons just as was the case for the

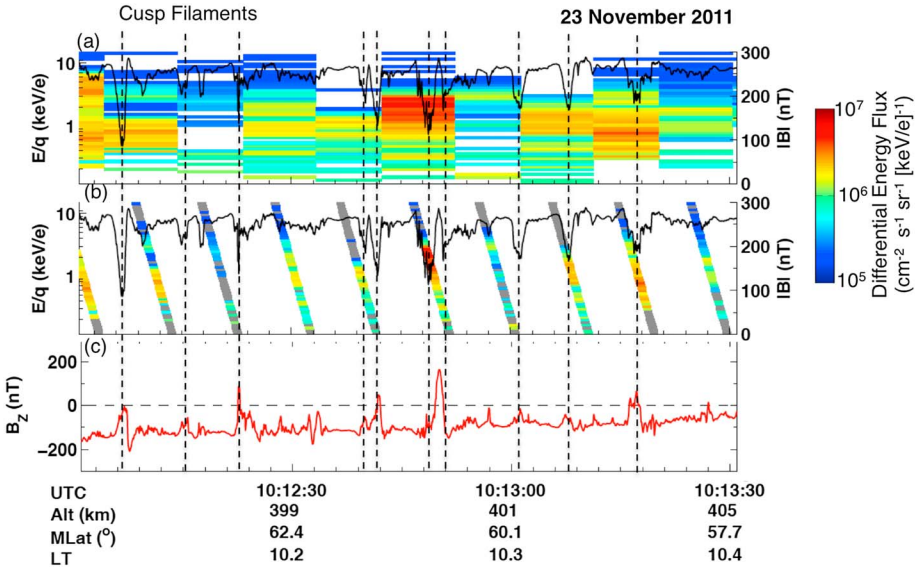

Figure 16. Illustration of cusp filaments (vertical dashed lines) recorded equatorward of the magnetospheric cusp on 23 November 2011. (a) Proton differential energy flux versus energy per charge and time. The intensity of the magnetic field is shown in black. (b) Differential flux versus energy per charge plotted at the time of each energy step. Because of a ramp up of high voltages on the FIPS electrostatic analyzer, there is an interval of several seconds at the beginning of each *E/q* scan when no data were collected. This ramp up manifests itself as gaps between scans. The effective FIPS duty cycle for this period was ~50%. The intensity of the magnetic field is again shown in black. (c) B_Z in MSM coordinates.

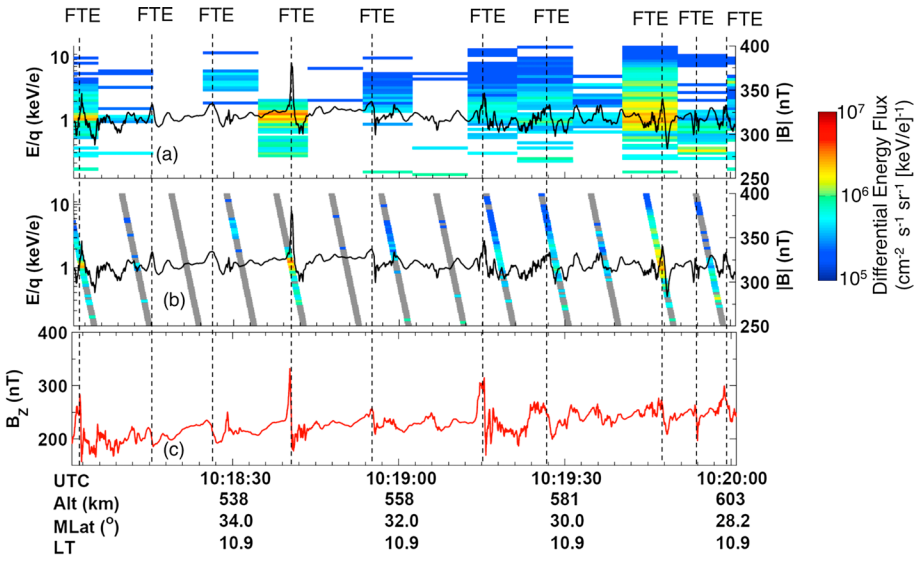

Figure 17. Illustration of flux transfer events (vertical dashed lines) recorded on approach to the magnetopause on 23 November 2011. (a) Proton differential energy flux versus energy per charge and time. The intensity of the magnetic field is shown in black. (b) Differential flux versus energy per charge plotted at the time of each energy step. Because of a ramp up of high voltages on the FIPS electrostatic analyzer, there is an interval of several seconds at the beginning of each *E/q* scan when no data were collected. This ramp up manifests itself as gaps between scans. The effective FIPS duty cycle for this period was ~50%. The intensity of the magnetic field is again shown in black. (c) B_Z in MSM coordinates.

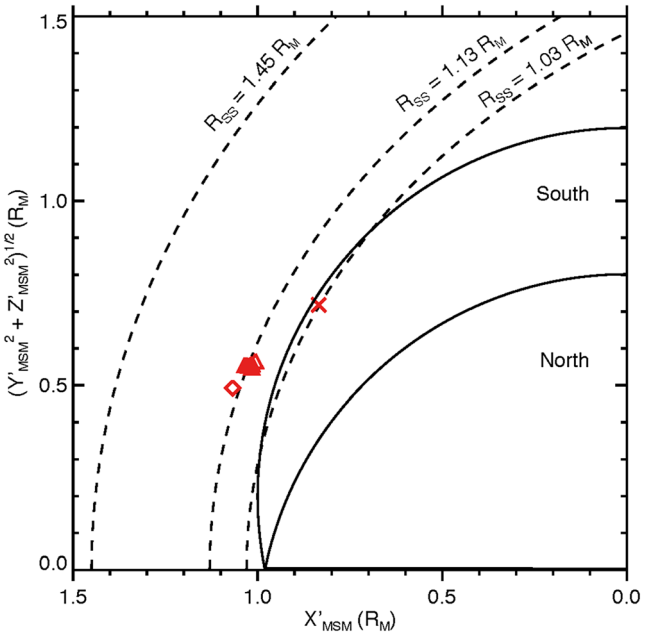

Figure 18. The location of the magnetopause during the extreme solar wind events of this study compared with the model magnetopause of *Winslow et al.* [2013]. The model magnetopause surface is displayed in aberrated cylindrical coordinates under mean (R_{ss} = 1.45 R_M) and extreme (R_{ss} = 1.13 or 1.03 R_M) solar wind pressure conditions. The magnetopause crossings on 23 November 2011, 8 May 2012, and 11 May 2012 are indicated with a diamond, cross, and triangles, respectively.

plasma filaments in the previous figure. The presence of protons with energies close to those observed in the magnetosheath is consistent with the FTEs being generated by magnetopause reconnection events.

6. Magnetopause Altitude Versus Solar Wind Pressure

We next consider the effect on Mercury's magnetopause location of the extreme solar wind conditions during the three events of this study. The magnetopause locations relative to Mercury during the three events, plotted in solar wind-aberrated cylindrical MSM coordinates, are shown in Figure 18. To estimate these locations, the shape of the magnetopause was assumed to have the general form determined by *Winslow et al.* [2013]. Their fit to a large ensemble of magnetopause crossings indicated a mean solar wind standoff distance of 1.45 R_M (Figure 18). Mercury's surface north of the magnetic equator, which is located at $Z'_{MSM} \sim 0.2\ R_M$, is shown separately from the surface south of the magnetic equator in Figure 18 to call attention to the strong effect of the dipole offset on magnetopause altitude (see also Figure 3).

For the magnetopause crossings on 23 November 2011 and 11 May 2012, the magnetopause locations cluster together and, as shown in Figure 18, are consistent with a solar wind standoff distance of about 1.13 R_M. The upstream solar wind dynamic pressures inferred from the analyses of these magnetopause crossings range from 44.3 to 53 nPa (Table 1). The reconnection rates determined from the magnetic field variations across the magnetopause range between 0.03 and 0.10 (Table 2).

In contrast, the magnetopause during the event of 8 May 2012 was located much closer to the planet, with a standoff distance of only 1.03 R_M (Figure 18). The upstream solar wind pressure and the reconnection rate determined for this magnetopause crossing are 65 nPa and 0.22, respectively. As shown in Figure 18, the combined effect of this high solar wind dynamic pressure and high dayside reconnection rate appear sufficient to bring the magnetopause into contact with the surface of Mercury at middle magnetic latitudes in the southern hemisphere.

The solar wind ram pressure at the subsolar point, P_{ss}, is plotted versus the solar wind standoff distance, R_{ss}, in Figure 19. From a large collection of magnetopause crossings recorded by MESSENGER during solar wind pressures between ~5 and 15 nPa, *Winslow et al.* [2013] determined a sixth-root relationship between P_{ss} and R_{ss} (Figure 19). This Earth-like relationship between upstream solar wind pressure and solar wind standoff distance implies that the magnetopause would be compressed down to the subsolar magnetic equator of Mercury when the upstream pressure reaches ~90 nPa.

However, Mercury is known to have an electrically conductive iron core that has a radius of ~2000 km [*Smith et al.*, 2012], a large fraction of Mercury's radius of 2440 km. As discussed above and illustrated in Figure 2, the compression of the dayside magnetosphere will induce electric currents in the outermost portion of Mercury's core that add to the closed magnetic flux in the dayside magnetosphere and temporarily increase the apparent magnetic moment of Mercury [*Hood and Schubert*, 1979; *Suess and Goldstein*, 1979].

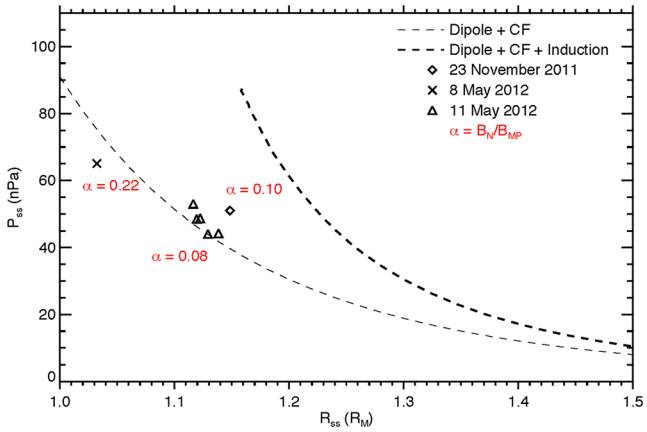

Figure 19. (a) Solar wind ram pressure, P_{SW}, versus extrapolated magnetopause standoff distance for the magnetopause crossings of this study. The magnetopause crossings on 23 November 2011, 8 May 2012, and 11 May 2012 are shown as a diamond, cross, and triangles, respectively. The dimensionless reconnection rate, α, averaged over the magnetopause crossings for each event, is also displayed for each event. The sixth-root relationship determined by *Winslow et al.* [2013] (thin dashed line) determined from a large data set of MESSENGER magnetopause encounters at typical upstream pressures of ~5 to 15 nPa is compared with a theoretical model that includes the effects of induction in Mercury's interior [*Glassmeier et al.*, 2007] (thick dashed line).

A predicted relationship between solar wind ram pressure and magnetopause standoff distance with the effects of induction included [*Glassmeier et al.*, 2007] is also shown in Figure 19. Models for the effect of induction on solar wind standoff distance at Mercury all predict that R_{ss} will be compressed below ~1.2 R_M only for solar wind pressures greater than ~90 nPa. However, as shown in Figure 19, individual magnetopause crossings during the extreme solar wind pressure events studied here were at distances as small as 1.03 R_M for solar wind pressures of only ~65 nPa.

The most likely reason for the proximity of the magnetopause to Mercury's surface during these events is the effect of reconnection and its transfer of magnetic flux into the tail [*Slavin and Holzer*, 1979]. In effect, dayside magnetic reconnection appears to be negating much of the shielding effect of the dayside induction currents during these extreme events. Indeed, the magnetopause crossings observed during the extreme solar wind events considered here fall approximately along the sixth-root, Chapman-Ferraro type pressure balance curve (thin dashed line in Figure 19), with the crossings at higher and lower reconnection rate lying ~(0.2–0.3) R_M closer and farther, respectively, from the offset dipole. These variations in magnetopause altitude suggest that, on average, the effects of erosion [*Slavin and Holzer*, 1979] and induction [*Hood and Schubert*, 1979] are in approximate balance. In this context, the magnetopause displacement to lower altitudes resulting from magnetic reconnection compensates for the increase in planetary moment caused by induction that acts to displace the magnetopause to higher altitudes. The induction still occurs, consistent with the high ram pressures, and still contributes to an enhanced planetary magnetic moment, but the location of the magnetopause for these extreme pressure events with strong magnetic reconnection is at lower altitudes than would be expected for induction alone.

7. Discussion

MESSENGER observations acquired during three extreme solar wind dynamic pressure events have been analyzed. Two events (23 November 2011 and 8 May 2012) were during coronal mass ejections (CMEs), and one (11 May 2012) was during a high-speed stream. The strength of the bow shock for the CME events was markedly weaker than for the high-speed stream event. The bow shock during the CME events was also more distant from Mercury than during the high-speed stream event. These facts argue that the solar wind Mach numbers for the CME events were much lower than for the high-speed stream event. The CME events also produced thick, low-β plasma depletion layers in the inner magnetosheath adjacent to the subsolar magnetopause. These PDLs are apparent in the low plasma densities and high temperatures measured by FIPS just outside of the magnetopause [see *Gershman et al.*, 2013, Figure 9]. The high-speed stream event, in contrast, produced a high-β magnetosheath and no plasma depletion layer. These conditions were reflected in both the large decrease in magnetic field intensity across the magnetopause and the high plasma densities measured by FIPS in the adjacent magnetosheath. The inferred solar wind pressures for all of these events are extreme, ~44 to 65 nPa compared with a mean value of 14.3 nPa for the MESSENGER mission [*Winslow et al.*, 2013].

When strong PDLs are present, such as was the case for the CME events studied here, the magnetic field intensity becomes nearly equal on both sides of the magnetopause. Under these conditions, reconnection is allowed for all nonzero magnetic shear angles, with the X line bisecting the planetary field inside of the magnetopause and the draped IMF in the external magnetosheath [*Sonnerup*, 1974; *Anderson et al*., 1997; *Eastwood et al*., 2013]. This situation is shown qualitatively for the events on 23 November 2011 and 8 May 2012, both characterized by low β and small to moderate shear, in Figures 20a and 20b. The draped IMF field lines (red) reconnect with the planetary field to create new merged field lines with the resultant "kink" 90° or less. In these cases the flow away from the extended X line was as much or more in the east and west directions as in the north and south directions. In contrast, the reconnected flux under the high-β, high-shear conditions associated with the high-speed stream on 11 May 2012 was much more kinked, and the flow away from the X line was largely in the north and south directions, as depicted in Figure 20c.

The reconnection rates determined from the component of the magnetic field normal to the magnetopause, i.e., 0.1–0.2, for the two CME events on 23 November 2011 and 8 May 2012, were comparable to or greater than the mean Mercury reconnection rates measured by *DiBraccio et al*. [2013]. They were also substantially greater than the 0.03–0.10 measured for the high-speed stream event. These results support recent inferences regarding relationships among low M_A, plasma β, magnetic shear angle, and reconnection rate at Mercury [*DiBraccio et al*., 2013; *Gershman et al*., 2013], and they also parallel recent developments regarding PDL formation under low M_A *Lavraud and Borovsky* [2008] and reconnection as a function of plasma β [*Phan et al*., 2013]. At Earth, the magnetosheath typically has high-β values, and this condition often limits fast reconnection to IMF orientations that have a southward component, i.e., magnetic shear angles across the magnetopause greater than 90° (the half-wave rectifier effect).

MESSENGER's observations of the northern cusp of Mercury during these three extreme solar wind events are displayed in Figures 20d–20f. During all of these extreme events, the northern cusp became unusually deep, with the average magnetic field intensity in the cusp dropping from ~300 nT to ~100 nT at MESSENGER altitudes as a result of the inflow of solar wind plasma from the magnetosheath. The cusps during 23 November 2011 and 11 May 2012 had similar poleward edges and centers, at magnetic latitudes 80–78° and 73–72°, respectively. The cusp during the 8 May 2012 periapsis pass was at markedly lower latitudes, from 70.5° to the equatorward edge at 57.9°. The central diamagnetic depression was centered at latitude 64.7°. The depth of the large-scale magnetic field decrease during the cusp crossing was greater than for the 23 November 2011 and 11 May 2012 events, with the minimum for 8 May 2012 less than ~20 nT.

At Earth, the depth and latitudinal extent of the diamagnetic decrease in the cusp are controlled by the rate of reconnection at the dayside magnetopause and just tailward of the cusp, as well as the dynamic pressure of the solar wind [*Reiff et al*., 1977; *Newell and Meng*, 1987; *Zhou et al*., 2000]. The fact that the diamagnetic signatures recorded in the cusp during these extreme events are much larger than the average values reported by *Winslow et al*. [2012] suggests that Mercury's cusp responds to increasing solar wind pressure in much the same manner as at Earth. The broadest and deepest of the three extreme cusps considered here is that for the 8 May 2012 event (Figure 20e). In agreement with expectations from observations at Earth, this event had the highest solar wind pressure and the highest reconnection rate at the dayside magnetopause. At Earth, equatorward displacements of the cusp are strongly correlated with southward IMF [*Burch*, 1973] and other predictors of dayside reconnection and energy input to the magnetosphere [*Newell et al*., 2007]. *Winslow et al*. [2012] did not observe a correlation between the north-south component of the IMF and the latitude of Mercury's cusp. However, it was later found by *DiBraccio et al*. [2013], and supported by the extreme events analyzed in this study, that the intensity of dayside reconnection at Mercury is primarily determined by M_A and the formation of low-β plasma depletion layers and not the north-south component of the upstream IMF. Hence, the fact that the 8 May 2012 event, which had the highest dayside reconnection rate of the three extreme events, occurred at the lowest magnetic latitude is in agreement with the result seen at Earth that dayside reconnection transfers magnetic flux to the magnetotail and reduces the latitude of the cusp. *Raines et al.* [2014] concluded that large fluxes of protons and planetary ions measured between the equatorward edge of the cusp and the magnetopause crossing were associated with dayside reconnection. The 23 November 2011 and 8 May 2012 events had the highest reconnection rates and contained the largest fluxes of ions at latitudes equatorward of the cusp, in agreement with their results.

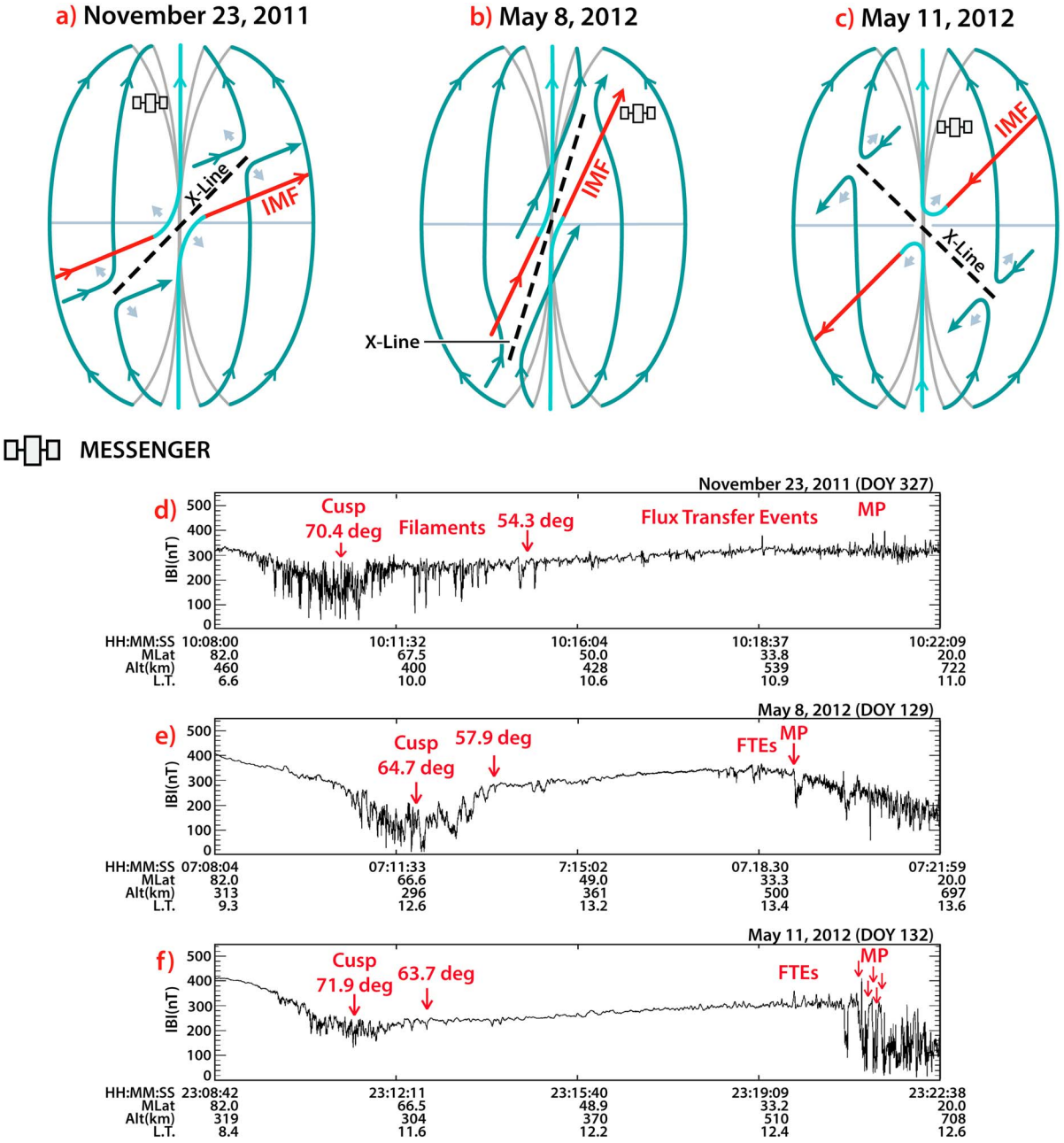

Figure 20. (a–c) Schematic illustrations of the direction of the IMF (red), planetary (green), and reconnected (red joined to green) magnetic flux tubes. The expected orientation of the reconnection X line (purple dashed line) and the Alfvénic flow out of the X line (short gray arrows) are also indicated. (d–f) Total magnetic field intensity versus time for the extreme solar wind passes, during the interval when MESSENGER was between magnetic latitudes 82°N and 20°N. The latitude of the center of the central magnetic cusp depression in |**B**| and the lowest latitude at which the narrow magnetic field depressions associated with plasma filaments were observed are indicated (red arrows). The locations of flux transfer events (FTEs) and magnetopause (MP) crossings are also labeled.

Flux transfer events are observed at most MESSENGER magnetopause crossings [*Slavin et al.*, 2009, 2010b, 2012a; *Imber et al.*, 2014], and they were seen for the three extreme solar wind intervals in Figures 20d–20f. However, the 23 November 2011 event stands out in that FTEs began to be observed at magnetic latitude ~ 50° and they continued until the magnetopause was crossed at 25.4°. The ~ 4 to 10 s quasiperiodicity of these events (see Figure 17) is very similar to the FTE shower events that *Slavin et al.* [2012a] reported tailward of the southern cusp. FTEs move in response to Maxwell stress as the newly reconnected flux tubes move toward a new equilibrium at the local Alfvén speed [*Cowley and Owen*, 1989]. Whether MESSENGER is well positioned to observe an FTE depends on the direction of the IMF and the location and extent of the X line(s) at which the FTE

is formed by reconnection [*Cooling et al*., 2001]. For the three extreme events considered here, schematic diagrams of X line locations, constructed on the basis of IMF orientation and spacecraft location (Figures 20a–20c), indicate that MESSENGER was properly positioned for observing FTEs moving away from extended low-latitude X line(s) on 23 November 2011 and 11 May 2012. Indeed, these are the two events for which FTE activity is the most widespread in Figures 20d–20f, with more and larger-amplitude FTEs observed for the 23 November 2011 event for which the reconnection rate at the magnetopause was measured to be greater. In contrast, the 8 May 2012 event, which had the highest magnetopause reconnection rate of the three, produced the fewest FTEs, and those seen were localized near the magnetopause crossing. However, inspection of Figure 20b shows that MESSENGER was not located in the central outflow region for tilted X line(s) passing through or near the subsolar point and so was much less likely to encounter FTEs. Hence, it appears that the reason for the small number of FTEs observed on 8 May 2012 may have been due to the location of MESSENGER rather than the rate at which FTEs were being produced during this event.

The 23 November 2012 event also revealed a new phenomenon, which we have termed a cusp plasma filament. As shown in Figure 16, these ~ 1–2 s long decreases in magnetic field intensity are located adjacent to and within the cusp, and the magnetic field intensity can drop from ~ 250 nT to ~ 20 nT during these brief events. However, these filaments were observed with decreasing amplitude as MESSENGER moved southward through the dayside magnetosphere and gradually gained altitude until reaching the magnetopause (Figures 3 and 10). A detailed analysis of these newly identified structures is beyond the scope of this study, but we note the qualitative similarities between our observations at Mercury and models developed to explain how plasma is injected into the magnetospheric cusp at Earth. In particular, the similarities between the 8 min repeat time of FTEs observed at the low-latitude magnetopause at Earth and dynamic changes in cusp auroral emissions and charged particle precipitation have been the basis for detailed models of ion acceleration and transport into the cusp by FTEs [*Menietti and Burch*, 1985; *Smith and Lockwood*, 1990]. The time resolution of the MESSENGER plasma measurements does not appear to be sufficient to test the predictions of these Earth-based models of cusp plasma injection at Mercury. However, the Earth models support our suggestion that the high-plasma-β filaments observed by MESSENGER near the cusp at Mercury may be due to FTE-associated injections of plasma.

From the large-scale diamagnetic decrease in magnetic field during cusp filament events, the ion flux to the surface at the cusps during the CME and high-speed stream events considered here should be an order of magnitude larger than under the quiet conditions described by *Winslow et al*. [2012]. This larger flux could result in an increased source rate to the exosphere via source processes that respond to ion flux. The best known of these processes is ion sputtering, the ejection of atoms and molecules from a surface following ion impact [*Sarantos et al*., 2007; *Killen et al*., 2001; *Wurz et al*., 2010]. Ions can also contribute to the exosphere indirectly via chemical sputtering [*Potter*, 1995] and ion-enhanced diffusion [*Killen et al*., 2001]. Both of these processes aid in freeing atoms from the crystal lattice so that they may be ejected by other processes, usually thermal desorption or ultraviolet photon-stimulated desorption. Recent modeling suggests that these indirect processes dominate over ion sputtering for the sodium exosphere [*Mura et al*., 2009; *Burger et al*., 2010; *Schmidt et al*., 2012].

Although MESSENGER's Mercury Atmospheric and Surface Composition Spectrometer Ultraviolet and Visible Spectrometer regularly observes Mercury's exosphere, the measurements taken during these extreme solar wind events were severely compromised by increased instrumental backgrounds induced by the higher flux of penetrating solar energetic particles. Further analysis is needed to determine if any signature of an exospheric response to these events can be reliably isolated from these large and variable backgrounds. Before MESSENGER orbital operations began, the inference that the exosphere responds to ion flux even during periods of relatively quiet space weather was made from a range of ground-based and MESSENGER flyby observations [*Potter and Morgan*, 1990; *McClintock et al*., 2008; *Leblanc et al*., 2009; *Vervack et a*l., 2010; *Benna et al*., 2010; *Burger et al*., 2010]. The orbital observations analyzed so far, however, have not shown the variability expected if the exosphere responds promptly to changes in ion flux. For example, *Winslow et al*. [2012] and *Raines et al*. [2013, 2014] reported a highly variable cusp and magnetosphere, but *Burger et al*. [2014] and *Cassidy et al*. [2012] found the exosphere to be highly stable as inferred from a lack of year-to-year variations in the observations. Such studies suggest that there is no simple correspondence between exospheric and magnetospheric activity. Much of the MESSENGER data set has yet to be analyzed, however, and further searches for exospheric responses to magnetospheric activity are warranted.

The three extreme solar wind intervals of this study with solar wind pressures of ~44 to 65 nPa, compared with the typical range of ~5–20 nPa [*Baker et al*., 2009, 2013; *Winslow et al*., 2013], reinforce the emerging picture of magnetospheric structure and dynamics at Mercury presented above. CMEs typically produce low M_A conditions, at least within their interior regions, and indeed, strong plasma depletion layers were observed for both of the two CME events analyzed here. Further examination of magnetopause structure for these two events (23 November 2011 and 8 May 2012) revealed high reconnection rates, 0.1–0.2, despite the small magnetic shear angles of only ~27 to 60° across the magnetopause. The high-speed stream produced a more Earth-like high-β magnetosheath and the large magnetic shear angles, ~148 to 166°, that would be expected to yield strong reconnection and possibly a major geomagnetic storm at Earth. However, only low reconnection rates, ~0.03 to 0.1, were determined from the magnetopause normal magnetic field component, most likely a result of the high plasma β in the magnetosheath. The relatively modest depth of the large-scale diamagnetic decrease in the cusp region supports our determination that the reconnection rate was lowest for the 11 May 2012 event.

8. Conclusions

This first study of Mercury's dayside magnetosphere during extreme solar wind conditions has revealed a number of important processes and facets to the system response. (1) Coronal mass ejections produce very strong plasma depletion layers, which support high rates of magnetopause reconnection independent of IMF orientation, in agreement with the results of *DiBraccio et al*. [2013] and *Gershman et al*. [2013]. (2) The magnetospheric cusp becomes deep and broad during these events, relative to the average conditions determined by *Winslow et al*. [2012] and *Raines et al*. [2014], presumably due to the high rate of dayside reconnection and the extreme solar wind pressure. (3) During one of these extreme events, quasiperiodic, large-amplitude FTEs were observed that strongly resemble the FTE showers along the high-latitude magnetopause reported by *Slavin et al*. [2012a]. (4) A newly recognized phenomenon, here termed cusp plasma filaments, was observed adjacent to and in the cusp proper; the cause of these filaments is not clear, but they may be the result of the same reconnection events that produce FTEs. (5) The subsolar magnetopause was observed at much lower altitudes during these extreme solar wind intervals than predicted by models that include the effects of induction in Mercury's interior [*Hood and Schubert*, 1979; *Glassmeier et al*., 2007]. We suggest that this difference is most likely the result of strong dayside reconnection and the reduction in magnetopause altitude that comes as a result of magnetic flux transfer to the magnetotail [*Slavin and Holzer*, 1979]. (6) For the 8 May 2012 event, which occurred during the largest solar wind pressure and exhibited the highest dayside reconnection rate, the magnetopause may have intersected the planetary surface in the southern hemisphere where Mercury's magnetic field is weakest.

Acknowledgments

We gratefully acknowledge the contribution of WSA-ENLIL simulations and graphic displays provided by P. J. Macneice and M. L. Mays of the Community Coordinated Modeling Center at the NASA Goddard Space Flight Center. Discussions with J. L. Burch concerning plasma injection into Earth's cusps are also acknowledged. CLJ and RMW acknowledge support from the Natural Sciences and Engineering Research Council of Canada, and CLJ acknowledges support from MESSENGER Participating Scientist grant NNX11AB84G. The MESSENGER project is supported by the NASA Discovery Program under contracts NASW-00002 to the Carnegie Institution of Washington and NAS5-97271 to The Johns Hopkins University Applied Physics Laboratory.

Yuming Wang thanks Tielong Zhang and another reviewer for their assistance in evaluating this paper.

References

Alexeev, I. I., E. S. Belenkaya, S. Y. Bobrovnikov, J. A. Slavin, and M. Sarantos (2008), Paraboloid model of Mercury, *J. Geophys. Res.*, *113*, A12210, doi:10.1029/2008JA013368.

Alexeev, I. I., et al. (2010), Mercury's magnetospheric magnetic field after the first two MESSENGER flybys, *Icarus*, *209*, 23–39, doi:10.1016/j.icarus.2010.01.024.

Anderson, B. J., T.-D. Phan, and S. A. Fuselier (1997), Relationships between plasma depletion and subsolar reconnection, *J. Geophys. Res.*, *102*, 9531–9542, doi:10.1029/97JA00173.

Anderson, B. J., M. H. Acuña, D. A. Lohr, J. Scheifele, A. Raval, H. Korth, and J. A. Slavin (2007), The Magnetometer instrument on MESSENGER, *Space Sci. Rev.*, *131*, 417–450, doi:10.1007/s11214-007-9246-7.

Anderson, B. J., M. H. Acuña, H. Korth, M. E. Purucker, C. L. Johnson, J. A. Slavin, S. C. Solomon, and R. L. McNutt Jr. (2008), The structure of Mercury's magnetic field from MESSENGER's first flyby, *Science*, *321*, 82–85.

Anderson, B. J., et al. (2010), The magnetic field of Mercury, *Space Sci. Rev.*, *152*, 307–339, doi:10.1007/s11214-009-9544-3.

Anderson, B. J., C. L. Johnson, H. Korth, M. E. Purucker, R. M. Winslow, J. A. Slavin, S. C. Solomon, R. L. McNutt Jr., J. M. Raines, and T. H. Zurbuchen (2011a), The global magnetic field of Mercury from MESSENGER orbital observations, *Science*, *333*, 1859–1862, doi:10.1126/science.

Anderson, B. J., J. A. Slavin, H. Korth, S. A. Boardsen, T. H. Zurbuchen, J. M. Raines, G. Gloeckler, R. L. McNutt Jr., and S. C. Solomon (2011b), The dayside magnetospheric boundary layer at Mercury, *Planet. Space Sci.*, *59*, 2037–2050.

Anderson, B. J., C. L. Johnson, H. Korth, R. M. Winslow, J. E. Borovsky, M. E. Purucker, J. A. Slavin, S. C. Solomon, M. T. Zuber, and R. L. McNutt Jr. (2012), Low-degree structure in Mercury's planetary magnetic field, *J. Geophys. Res.*, *117*, E00L12, doi:10.1029/2012JE004159.

Andrews, G. B., et al. (2007), The Energetic Particle and Plasma Spectrometer instrument on the MESSENGER spacecraft, *Space Sci. Rev.*, *131*, 523–556, doi:10.1007/s11214-007-9272-5.

Arge, C. N., J. G. Luhmann, D. Odstrcil, C. J. Schrijver, and Y. Li (2004), Stream structure and coronal sources of the solar wind during the May 12th, 1997 CME, *J. Atmos. Solar Terr. Phys.*, *66*, 1295–1309.

Aubry, M. P., M. G. Kivelson, and C. T. Russell (1971), Motion and structure of the magnetopause, *J. Geophys. Res.*, *76*, 1673–1696, doi:10.1029/JA076i007p01673.

Baker, D. N., T. I. Pulkkinen, V. Angelopoulos, W. Baumjohann, and R. L. McPherron (1996), Neutral line model of substorms: Past results and present view, *J. Geophys. Res.*, *101*, 12,975–13,010, doi:10.1029/95JA03753.
Baker, D. N., et al. (2009), Space environment of Mercury at the time of the first MESSENGER flyby: Solar wind and interplanetary magnetic field modeling of upstream conditions, *J. Geophys. Res.*, *114*, A10101, doi:10.1029/2009JA014287.
Baker, D. N., et al. (2013), Solar wind forcing at Mercury: WSA-ENLIL model results, *J. Geophys. Res. Space Physics*, *118*, 45–57, doi:10.1029/2012JA018064.
Benna, M., et al. (2010), Modeling of the magnetosphere of Mercury at the time of the first MESSENGER flyby, *Icarus*, *209*, 3–10, doi:10.1016/j.icarus.2009.11.036.
Berchem, J., and C. T. Russell (1982), The thickness of the magnetopause current layer: ISEE 1 and 2 observations, *J. Geophys. Res.*, *87*, 2108–2114, doi:10.1029/JA087iA04p02108.
Burch, J. L. (1973), Rate of erosion of dayside magnetic flux based on a quantitative study of the dependence of polar cusp latitude on the interplanetary magnetic field, *Radio Sci.*, *8*, 955–961, doi:10.1029/RS008i011p00955.
Burger, M. H., et al. (2010), Monte Carlo modeling of sodium in Mercury's exosphere during the first two MESSENGER flybys, *Icarus*, *209*, 63–74, doi:10.1016/j.icarus.2010.05.007.
Burger, M. H., R. M. Killen, W. E. McClintock, A. W. Merkel, R. J. Vervack Jr., T. A. Cassidy, and M. Sarantos (2014), Seasonal variations in Mercury's dayside calcium exosphere, *Icarus*, *238*, 51–58.
Burton, R. K., R. L. McPherron, and C. T. Russell (1975), The terrestrial magnetosphere: A half-wave rectifier of the interplanetary electric field, *Science*, *189*, 717–718.
Caan, M. N., R. L. McPherron, and C. T. Russell (1977), Characteristics of the association between the interplanetary magnetic field and substorms, *J. Geophys. Res.*, *82*, 4837–4842, doi:10.1029/JA082i029p04837.
Cassidy, T. A., A. W. Merkel, M. H. Burger, W. E. McClintock, R. M. Killen, M. Sarantos, A. L. Sprague, R. J. Vervack Jr., and S. C. Solomon (2012), Mercury's seasonal sodium exosphere, *EPSC Abstracts*, *7*, abstract EPSC2012-766.
Cooling, B. M. A., C. J. Owen, and S. J. Schwartz (2001), Role of the magnetosheath flow in determining the motion of open flux tubes, *J. Geophys. Res.*, *106*, 18,763–18,776, doi:10.1029/2000JA000455.
Cowley, S. W. H., and C. J. Owen (1989), A simple illustrative model of open flux tube motion over the dayside magnetopause, *Planet. Space Sci.*, *37*, 1461–1475.
Crooker, N. U. (1979), Dayside merging and cusp geometry, *J. Geophys. Res.*, *84*, 951–959, doi:10.1029/JA084iA03p00951.
DiBraccio, G. A., J. A. Slavin, S. A. Boardsen, B. J. Anderson, H. Korth, T. H. Zurbuchen, J. M. Raines, D. N. Baker, R. L. McNutt Jr., and S. C. Solomon (2013), MESSENGER observations of magnetopause structure and dynamics at Mercury, *J. Geophys. Res. Space Physics*, *118*, 997–1008, doi:10.1002/jgra.50123.
Dungey, J. W. (1961), Interplanetary magnetic field and the auroral zones, *Phys. Rev. Lett.*, *6*, 47–48, doi:10.1103/*PhysRevLett*.6.47.
Eastwood, J. P., T. D. Phan, M. Oieroset, M. A. Shay, K. Malakit, M. Swisdak, J. F. Drake, and A. Masters (2013), Influence of asymmetries and guide fields on the magnetic reconnection diffusion region in collisionless space plasmas, *Plasma Phys. Control. Fusion*, *55*, 124001, doi:10.1088/0741-3335/55/12/124001.
Farrugia, C. J., N. V. Erkaev, H. K. Biernat, and L. F. Burlaga (1995), Anomalous magnetosheath properties during Earth passage of an interplanetary magnetic cloud, *J. Geophys. Res.*, *10*, 19,245–19,257, doi:10.1029/95JA0108.
Fuselier, S. A., and W. S. Lewis (2011), Properties of near-Earth magnetic reconnection from in-situ observations, *Space Sci. Rev.*, *160*, 95–121, doi:10.1007/s11214-011-9820-x.
Gershman, D. J., J. A. Slavin, J. M. Raines, T. H. Zurbuchen, B. J. Anderson, H. Korth, D. N. Baker, and S. C. Solomon (2013), Magnetic flux pileup and plasma depletion in Mercury's subsolar magnetosheath, *J. Geophys. Res. Space Physics*, *118*, 7181–7199, doi:10.1002/2013JA019244.
Gershman, D. J., J. A. Slavin, J. M. Raines, T. H. Zurbuchen, B. J. Anderson, H. Korth, D. N. Baker, and S. C. Solomon (2014), Ion kinetic properties in Mercury's pre-midnight plasma sheet, *Geophys. Res. Lett.*, *41*, doi:10.1002/2014GL060468.
Glassmeier, K.-H. (2000), Currents in Mercury's magnetosphere, in *Magnetospheric Current Systems*, *Geophys. Monogr. Ser.*, vol. 118, edited by S. Ohtani et al., pp. 371–380, AGU, Washington, D. C.
Glassmeier, K.-H., J. Grosser, U. Auster, D. Constantinescu, Y. Narita, and S. Stellmach (2007), Electromagnetic induction effects and dynamo action in the Hermean system, *Space Sci. Rev.*, *132*, 511–527, doi:10.1007/s11214-007-9244-9.
Gosling, J. T., et al. (2005), Direct evidence for magnetic reconnection in the solar wind near 1 AU, *J. Geophys. Res.*, *110*, A01107, doi:10.1029/2004JA010809.
Grosser, J., K.-H. Glassmeier, and A. Stadelmann (2004), Induced magnetic field effects at planet Mercury, *Planet. Space Sci.*, *52*, 1251–1260.
Hasegawa, H., B. U. Ö. Sonnerup, C. J. Owen, B. Klecker, G. Paschmann, A. Balogh, and H. Rème (2006), The structure of flux transfer events recovered from Cluster data, *Ann. Geophys.*, *24*, 603–618, doi:10.5194/angeo-24-603-2006.
Hasegawa, H., et al. (2010), Evidence for a flux transfer event generated by multiple X-line reconnection at the magnetopause, *Geophys. Res. Lett.*, *37*, L16101, doi:10.1029/2010GL044219.
Hill, T. W., A. J. Dessler, and R. A. Wolf (1976), Mercury and Mars: The role of ionospheric conductivity in the acceleration of magnetospheric particles, *Geophys. Res. Lett.*, *3*, 429–432, doi:10.1029/GL003i008p00429.
Holzer, R. E., and J. A. Slavin (1978), Magnetic flux transfer associated with expansions and contractions of the dayside magnetosphere, *J. Geophys. Res.*, *83*, 3831–3839, doi:10.1029/JA083iA08p03831.
Hood, L. L., and G. Schubert (1979), Inhibition of solar wind impingement on Mercury by planetary induction currents, *J. Geophys. Res.*, *84*, 2641–2647, doi:10.1029/JA084iA06p02641.
Huang, C.-S., A. D. DeJong, and X. Cai (2009), Magnetic flux in the magnetotail and polar cap during sawteeth, isolated substorms, and steady magnetospheric convection events, *J. Geophys. Res.*, *114*, A07202, doi:10.1029/2009JA014232.
Imber, S. M., J. A. Slavin, S. A. Boardsen, B. J. Anderson, H. Korth, R. L. McNutt Jr., and S. C. Solomon (2014), MESSENGER observations of large dayside flux transfer events: Do they drive Mercury's substorm cycle?, *J. Geophys. Res. Space Physics*, *119*, 5613–5623, doi:10.1002/2014JA019884.
Johnson, C. L., et al. (2012), MESSENGER observations of Mercury's magnetic field structure, *J. Geophys. Res.*, *117*, E00L14, doi:10.1029/2012JE004217.
Killen, R. M., et al. (2001), Evidence for space weather at Mercury, *J. Geophys. Res.*, *106*, 20,509–20,525, doi:10.1029/2000JE001401.
Lavraud, B., and J. E. Borovsky (2008), Altered solar wind–magnetosphere interaction at low Mach numbers: Coronal mass ejections, *J. Geophys. Res.*, *113*, A00B08, doi:10.1029/2008JA013192.
Leblanc, F., et al. (2009), Short-term variations of Mercury's Na exosphere observed with very high spectral resolution, *Geophys. Res. Lett.*, *36*, L07201, doi:10.1029/2009GL038089.
Lee, L. C., and Z. F. Fu (1985), A theory of magnetic flux transfer at the Earth's magnetopause, *Geophys. Res. Lett.*, *12*, 105–108.

Masters, A., J. A. Slavin, G. A. DiBraccio, T. Sundberg, R. M. Winslow, C. L. Johnson, B. J. Anderson, and H. Korth (2013), A comparison of magnetic overshoots at the bow shocks of Mercury and Saturn, *J. Geophys. Res. Space Physics*, *118*, 4381–4390, doi:10.1002/jgra.50428.

McClintock, W. E., et al. (2008), Spectroscopic observations of Mercury's surface reflectance during MESSENGER's first Mercury flyby, *Science*, *321*, 62–65, doi:10.1126/science.1159933.

McPherron, R. L., C. T. Russell, and M. P. Aubry (1973), Satellite studies of magnetospheric substorms on August 15, 1968: 9. Phenomenological model for substorms, *J. Geophys. Res.*, *78*, 3131–3149, doi:10.1029/JA078i016p03131.

Menietti, J. D., and J. L. Burch (1985), Spatial extent of the plasma injection region in the cusp–magnetosheath interface, *J. Geophys. Res.*, *93*, 5345–5351, doi:10.1029/JA093iA01p00105.

Milan, S. E., S. W. H. Cowley, M. Lester, D. M. Wright, J. A. Slavin, M. Fillingim, C. W. Carlson, and H. J. Singer (2004), Response of the magnetotail to changes in the open flux content of the magnetosphere, *J. Geophys. Res.*, *109*, A04220, doi:10.1029/2003JA010350.

Mozer, F. S., and A. Hull (2010), Scaling the energy conversion rate from magnetic field reconnection to different bodies, *Phys. Plasmas*, *17*, 102906, doi:10.1063/1.3504224.

Mozer, F. S., and A. Retinò (2007), Quantitative estimates of magnetic field reconnection properties from electric and magnetic field measurements, *J. Geophys. Res.*, *112*, A10206, doi:10.1029/2007JA012406.

Müller, J., S. Simon, Y.-C. Wang, U. Motschmann, D. Heyner, J. Schüle, W.-H. Ip, G. Kleindienst, and G. J. Pringle (2012), Origin of Mercury's double magnetopause: 3D hybrid simulation study with A.I.K.E.F., *Icarus*, *218*, 666–687, doi:10.1016/j.icarus.2011.12.028.

Mura, A., P. Wurz, H. I. M. Lichtenegger, H. Schleicher, H. Lammer, D. Delcourt, A. Milillo, S. Massetti, M. L. Khodachenko, and S. Orsini (2009), The sodium exosphere of Mercury: Comparison between observations during Mercury's transit and model results, *Icarus*, *200*, 1–11, doi:10.1016/j.icarus.2008.11.014.

Ness, N. F., K. W. Behannon, R. P. Lepping, Y. C. Wang, and K. H. Schatten (1974), Observations of magnetic field near Mercury: Preliminary results from Mariner 10, *Science*, *185*, 151–159.

Ness, N. F., K. W. Behannon, R. P. Lepping, and Y. C. Whang (1976), Observations of Mercury's magnetic field, *Icarus*, *28*, 479–488.

Newell, P. T., and C.-I. Meng (1987), Cusp width and B_z: Observations and a conceptual model, *J. Geophys. Res.*, *92*, 13,673–13,678, doi:10.1029/JA092iA12p13673.

Newell, P. T., T. Sotirelis, K. Liou, C.-I. Meng, and F. J. Rich (2007), A nearly universal solar wind-magnetosphere coupling function inferred from 10 magnetospheric state variables, *J. Geophys. Res.*, *112*, A01206, doi:10.1029/2006JA012015.

Odstrcil, D., P. Riley, and X. P. Zhao (2004), Numerical simulation of the 12 May 1997 interplanetary CME event, *J. Geophys. Res.*, *109*, A02116, doi:10.1029/2003JA010135.

Owen, C. J., A. Marchaudon, M. W. Dunlop, A. N. Fazakerley, J.-M. Bosqued, J. P. Dewhurst, R. C. Fear, S. A. Fuselier, A. Balogh, and H. Rèmy (2008), Cluster observations of "crater" flux transfer events in the dayside high-latitude magnetopause, *J. Geophys. Res.*, *113*, A07S04, doi:10.1029/2007JA012701.

Paschmann G., M. Oieroset, and T. Phan (2013), In-situ observations of reconnection in space, *Space Sci. Rev.*, *178*, 385–417, doi:10.1007/s11214-012-9957-2.

Phan, T. D., et al. (2005), A magnetic reconnection X-line extending more than 390 Earth radii in the solar wind, *Nature*, *439*, 175–178, doi:10.1038/nature04393.

Phan, T. D., G. Paschmann, J. T. Gosling, M. Oieroset, M. Fujimoto, J. P. Drake, and V. Angelopoulos (2013), The dependence of magnetic reconnection on plasma β and magnetic shear: Evidence from magnetopause observations, *Geophys. Res. Lett.*, *40*, 11–16, doi:10.1029/2012GL054528.

Potter, A. E. (1995), Chemical sputtering could produce sodium vapor and ice on Mercury, *Geophys. Res. Lett.*, *22*, 3289–3292, doi:10.1029/95GL03181.

Potter, A. E., and T. H. Morgan (1990), Evidence for magnetospheric effects on the sodium atmosphere of Mercury, *Science*, *248*, 835–838, doi:10.1126/science.248.4957.835.

Raeder, J. (2006), Flux transfer events: 1. Generation mechanism for strong southward IMF, *Ann. Geophys.*, *24*, 381–392, doi:10.5194/angeo-24-381-2006.

Raines, J. M., J. A. Slavin, T. H. Zurbuchen, G. Gloeckler, B. J. Anderson, D. N. Baker, H. Korth, S. M. Krimigis, and R. L. McNutt Jr. (2011), MESSENGER observations of the plasma environment near Mercury, *Planet. Space Sci.*, *59*, 2004–2015, doi:10.1016/j.pss.2011.02.004.

Raines, J. M., et al. (2013), Distribution and compositional variations of plasma ions in Mercury's space environment: The first three Mercury years of MESSENGER observations, *J. Geophys. Res. Space Physics*, *118*, 1604–1619, doi:10.1029/2012JA018073.

Raines, J. M., D. J. Gershman, J. A. Slavin, T. H. Zurbuchen, H. Korth, B. J. Anderson, G. Gloeckler, and S. C. Solomon (2014), Structure and dynamics of Mercury's magnetospheric cusp: MESSENGER measurements of protons and planetary ions, *J. Geophys. Res. Space Physics*, *119*, doi:10.1002/2014JA020120.

Reiff, P. H., and J. G. Luhmann (1986), Solar wind control of the polar-cap potential, in *Solar Wind-Magnetosphere Coupling*, edited by Y. Kamide and J. A. Slavin, pp. 453–476, Terra Scientific, Tokyo, Japan.

Reiff, P. H., T. W. Hill, and J. L. Burch (1977), Solar wind plasma injection at the dayside magnetospheric cusp, *J. Geophys. Res.*, *82*, 479–491, doi:10.1029/JA082i004p00479.

Richardson, J. D. (2002), The magnetosheaths of the outer planets, *Planet. Space Sci.*, *50*, 503–517.

Rijnbeek, R. P., S. W. H. Cowley, D. J. Southwood, and C. T. Russell (1984), A survey of dayside flux transfer events observed by ISEE-1 and ISEE-2 magnetometers, *J. Geophys. Res.*, *89*, 786–800, doi:10.1029/JA089iA02p00786.

Russell, C. T. (1977), On the relative locations of the bow shocks of the terrestrial planets, *Geophys. Res. Lett.*, *4*, 387–390, doi:10.1029/GL004i010p00387.

Russell, C. T., and R. C. Elphic (1978), Initial ISEE magnetometer results: Magnetopause observations, *Space Sci. Res.*, *22*, 681–715.

Russell, C. T., and R. J. Walker (1985), Flux transfer events at Mercury, *J. Geophys. Res.*, *90*, 11,067–11,074, doi:10.1029/JA090iA11p11067.

Sarantos, M., and J. A. Slavin (2009), On the possible formation of Alfven wings at Mercury during encounters with coronal mass ejections, *Geophys. Res. Lett.*, *36*, L04107, doi:10.1029/2008GL036747.

Sarantos, M., R. M. Killen, and D. Kim (2007), Predicting the long-term solar wind ion-sputtering source at Mercury, *Planet. Space Sci.*, *55*, 1584–1595, doi:10.1016/j.pss.2006.10.011.

Schmidt, C. A., J. Baumgardner, M. Mendillo, and J. K. Wilson (2012), Escape rates and variability constraints for high-energy sodium sources at Mercury, *J. Geophys. Res.*, *117*, A03301, doi:10.1029/2011JA017217.

Scurry, L., C. T. Russell, and J. T. Gosling (1994), Geomagnetic activity and the beta dependence of the dayside reconnection rate, *J. Geophys. Res.*, *99*, 14,811–14,814, doi:10.1029/94JA00794.

Sergeev, V., R. J. Pellenin, and T. I. Pulkkinen (1996), Steady magnetospheric convection: A review of recent results, *Space Sci. Rev.*, *75*, 551–604.

Shue, J.-H., J. K. Chao, H. C. Fu, C. T. Russell, P. Song, K. K. Khurana, and H. J. Singer (1997), A new functional form to study the solar wind control of the magnetopause size and shape, *J. Geophys. Res.*, *102*, 9497–9511, doi:10.1029/97JA00196.

Sibeck, D. G., R. E. Lopez, and E. C. Roelof (1991), Solar wind control of the magnetopause shape, location, and motion, *J. Geophys. Res.*, *96*, 5489–5495, doi:10.1029/90JA02464.

Siscoe, G., and L. Christopher (1975), Variations in the solar wind stand-off distance at Mercury, *Geophys. Res. Lett.*, *2*, 158–160, doi:10.1029/GL002i004p00158.

Siscoe, G. L., N. F. Ness, and C. M. Yeates (1975), Substorms on Mercury?, *J. Geophys. Res.*, *80*, 4359–4363, doi:10.1029/JA080i031p04359.

Slavin, J. A., and R. E. Holzer (1979), The effect of erosion on the solar wind stand-off distance at Mercury, *J. Geophys. Res.*, *84*, 2076–2082, doi:10.1029/JA084iA05p02076.

Slavin, J. A., R. E. Holzer, J. R. Spreiter, and S. S. Stahara (1984), Planetary Mach cones: Theory and observation, *J. Geophys. Res.*, *89*, 2708–2714, doi:10.1029/JA089iA05p02708.

Slavin, J. A., R. P. Lepping, J. Gjerloev, D. H. Fairfield, M. Hesse, C. J. Owen, M. B. Moldwin, T. Nagai, A. Ieda, and T. Mukai (2003), Geotail observations of magnetic flux ropes in the plasma sheet, *J. Geophys. Res.*, *108*(A1), 1015, doi:10.1029/2002JA009557.

Slavin, J. A., et al. (2008), Mercury's magnetosphere after MESSENGER's first flyby, *Science*, *321*, 85–89.

Slavin, J. A., et al. (2009), MESSENGER observations of magnetic reconnection in Mercury's magnetosphere, *Science*, *324*, 606–610.

Slavin, J. A., et al. (2010a), MESSENGER observations of extreme loading and unloading of Mercury's magnetic tail, *Science*, *329*, 665–668.

Slavin, J. A., et al. (2010b), MESSENGER observations of large flux transfer events at Mercury, *Geophys. Res. Lett.*, *37*, L02105, doi:10.1029/2009GL041485.

Slavin, J. A., et al. (2012a), MESSENGER observations of a flux-transfer-event shower at Mercury, *J. Geophys. Res.*, *117*, A00M06, doi:10.1029/2012JA017926.

Slavin, J. A., et al. (2012b), MESSENGER and Mariner 10 flyby observations of magnetotail structure and dynamics at Mercury, *J. Geophys. Res.*, *117*, A01215, doi:10.1029/2011JA016900.

Smith, D. E., et al. (2012), Gravity field and internal structure of Mercury from MESSENGER, *Science*, *336*, 214–217.

Smith, M. F., and M. Lockwood (1990), The statistical cusp: A flux transfer event model, *Geophys. Res. Lett.*, *17*, 1069–1072, doi:10.1029/GL017i008p01069.

Solomon, S. C., et al. (2001), The MESSENGER mission to Mercury: Scientific objectives and implementation, *Planet. Space Sci.*, *49*, 1445–1465, doi:10.1016/S0032-0633(01)00085-X.

Sonnerup, B. U. Ö. (1974), Magnetopause reconnection rate, *J. Geophys. Res.*, *79*, 1546–1549, doi:10.1029/JA079i010p01546.

Sonnerup, B. U. Ö., and L. J. Cahill Jr. (1967), Magnetopause structure and attitude from Explorer 12 observations, *J. Geophys. Res.*, *72*, 171–183, doi:10.1029/JZ072i001p00171.

Sonnerup, B. U. Ö., G. Paschmann, I. Papamastorakis, N. Sckopke, G. Haerendel, S. J. Bame, J. R. Asbridge, J. T. Gosling, and C. T. Russell (1981), Evidence for magnetic field reconnection at the Earth's magnetopause, *J. Geophys. Res.*, *86*, 10,049–10,067, doi:10.1029/JA086iA12p10049.

Spreiter, J. R., A. L. Summers, and A. Y. Alksne (1966), Hydromagnetic flow around the magnetosphere, *Planet. Space Sci.*, *14*, 223–253.

Suess, S. T., and B. E. Goldstein (1979), Compression of the Hermean magnetosphere by the solar wind, *J. Geophys. Res.*, *84*, 3306–3312, doi:10.1029/JA084iA07p03306.

Sundberg, T., et al. (2012), MESSENGER observations of dipolarization events in Mercury's magnetotail, *J. Geophys. Res.*, *117*, A00M03, doi:10.1029/2012JA017756.

Tanskanen, E. I. (2009), A comprehensive high-throughput analysis of substorms observed by IMAGE magnetometer network: Years 1993–2003 examined, *J. Geophys. Res.*, *114*, A05204, doi:10.1029/2008JA013682.

Tanskanen, E., J. A. Slavin, D. H. Fairfield, D. G. Sibeck, J. Gjerloev, T. Mukai, A. Ieda, and T. Nagai (2005), Response of the magnetotail to prolonged southward B_z intervals: Loading, unloading, and continuous dissipation, *J. Geophys. Res.*, *110*, A03216, doi:10.1029/2004JA010561.

Toth, G., and D. Odstrcil (1996), Comparison of some flux corrected transport and total variation diminishing numerical schemes for hydrodynamic and magnetohydrodynamic problems, *J. Comp. Phys.*, *128*, 82–100.

Vervack, R. J., Jr., et al. (2010), Mercury's complex exosphere: Results from MESSENGER's third flyby, *Science*, *329*, 672–675, doi:10.1126/science.1188572.

Wang, Y. L., et al. (2005), Initial results of high-latitude magnetopause and low-latitude flank flux transfer events from 3 years of Cluster observations, *J. Geophys. Res.*, *110*, A11221, doi:10.1029/2005JA011150.

Winslow, R. M., C. L. Johnson, B. J. Anderson, H. Korth, J. A. Slavin, M. E. Purucker, and S. C. Solomon (2012), Observations of Mercury's northern cusp with MESSENGER's Magnetometer, *Geophys. Res. Lett.*, *39*, L08112, doi:10.1029/2012GL051472.

Winslow, R. M., B. J. Anderson, C. L. Johnson, J. A. Slavin, H. Korth, M. E. Purucker, D. N. Baker, and S. C. Solomon (2013), Mercury's magnetopause and bow shock from MESSENGER Magnetometer observations, *J. Geophys. Res. Space Physics*, *118*, 2213–2227, doi:10.1002/jgra.50237.

Wurz, P., J. A. Whitby, U. Rohner, J. A. Martín-Fernández, H. Lammer, and C. Kolb (2010), Self-consistent modelling of Mercury's exosphere by sputtering, micro-meteorite impact and photon-stimulated desorption, *Planet. Space Sci.*, *58*, 1599–1616, doi:10.1016/j.pss.2010.08.003.

Xie, H., L. Ofman, and G. Lawrence (2004), Cone model for halo CMEs: Application to space weather forecasting, *J. Geophys. Res.*, *109*, A03109, doi:10.1029/2003JA010226.

Zhang, H., K. K. Khurana, M. G. Kivelson, V. Angelopoulos, Z. Y. Pu, Q.-G. Zong, J. Liu, and X.-Z. Zhou (2008), Modeling a force-free flux transfer event probed by multiple THEMIS spacecraft, *J. Geophys. Res.*, *113*, A00C05, doi:10.1029/2008JA013451.

Zhou, X.-W., and C. T. Russell (1997), The location of the high-latitude polar cusp and the shape of the surrounding magnetopause, *J. Geophys. Res.*, *102*, 105–110, doi:10.1029/96JA02702.

Zhou, X.-W., C. T. Russell, G. Le, S. A. Fuselier, and J. D. Scudder (2000), Solar wind control of the polar cusp at high latitude, *J. Geophys. Res.*, *105*, 245–251, doi:10.1029/1999JA900412.

Zurbuchen, T. H., J. M. Raines, G. Gloeckler, S. M. Krimigis, J. A. Slavin, P. L. Koehn, R. M. Killen, A. L. Sprague, R. L. McNutt Jr., and S. C. Solomon (2008), MESSENGER observations of the composition of Mercury's ionized exosphere and plasma environment, *Science*, *321*, 90–92, doi:10.1126/science.1159314.

Zwan, B. J., and R. A. Wolf (1976), Depletion of solar wind plasma near a planetary boundary, *J. Geophys. Res.*, *81*, 1636–1648, doi:10.1029/JA081i010p01636.